NACA RM E54H20

NACA

RESEARCH MEMORANDUM

METHOD OF DESIGNING CORRUGATED SURFACES HAVING MAXIMUM COOLING EFFECTIVENESS WITHIN PRESSURE-DROP LIMITATIONS FOR APPLICATION TO COOLED TURBINE BLADES

By Henry O. Slone, James E. Hubbartt, and Vernon L. Arne

Lewis Flight Propulsion Laboratory
Cleveland, Ohio

NATIONAL ADVISORY COMMITTEE
FOR AERONAUTICS

WASHINGTON
December 9, 1954

NATIONAL ADVISORY COMMITTEE FOR AERONAUTICS

RESEARCH MEMORANDUM

METHOD OF DESIGNING CORRUGATED SURFACES HAVING MAXIMUM COOLING EFFECTIVENESS WITHIN PRESSURE-DROP LIMITATIONS FOR APPLICATION TO COOLED TURBINE BLADES

By Henry O. Slone, James E. Hubbartt, and Vernon L. Arne

SUMMARY

A method utilizing charts is presented for the systematic determination of a corrugation geometry configuration which, for a specific application to an air-cooled turbine blade, gives the required amount of blade temperature reduction using the minimum amount of coolant flow within pressure-drop limitations. The cooling effectiveness varies appreciably with changes in corrugation geometry which may be reflected in improvements in the coolant flow and pressure requirements for air-cooled turbine blades.

A numerical example is included to illustrate the use of the method. The details of the derivations of the equations and charts are also included.

INTRODUCTION

A good air-cooled turbine blade requires a design which, for a specific application, will give the required amount of blade temperature reduction with the minimum amount of coolant flow and still be within pressure-drop and fabrication limits. An analytical investigation was undertaken to develop a reliable method for the selection and evaluation of corrugated-type coolant passage configurations for convection-cooled blades.

The effectiveness of convection cooling can be greatly augmented by additional heat-transfer surface in the form of fins. A practical type of fin is a corrugated surface brazed to a wall or sheet. At the present time, air-cooled blades having internal heat-transfer surfaces of the corrugated type are promising because of (1) the high heat-transfer effectiveness of corrugated surfaces (ref. 1), (2) the ease of fabrication and freedom in selection of corrugation height or amplitude, gage or thickness, and spacing, (3) corrugated surfaces can serve as structural

elements, and (4) corrugations of uniform height, along with a blade insert, give a more uniform peripheral distribution of the coolant. The application of corrugated surfaces to air-cooled turbine blades has been investigated to some extent in reference 1 wherein air-cooled corrugated blades were compared with air-cooled blades having other types of surfaces. An experimental investigation conducted in a modified turbojet engine to determine the cooling effectiveness of an air-cooled corrugated rotor blade is reported in reference 2. In addition, experimental tests of heat exchanger cores using corrugated surfaces are described in references 3 and 4.

Reference 1 presents analytical methods whereby a single corrugation geometry configuration may be analyzed on the basis of cooling effectiveness and pressure-drop limitations. However, no systematic procedure is available for investigating a number of different corrugation geometry combinations in order to select the best combination for a given application. Consequently, a method using available theoretical relations for heat transfer and pressure drop was evolved which enables the designer to investigate in a relatively short time a number of corrugation geometry combinations for any specific application. This method may be used to design an air-cooled turbine blade with an internal coolant passage containing a corrugation geometry which gives for the application under consideration the best combination of (1) high heat-transfer effectiveness and (2) the lowest possible coolant flow within pressure-drop limitations. This report presents charts which relate the corrugation geometry and coolant flow to the effective inside heat-transfer coefficient and describes in detail the use of these relations in the selection of a corrugation geometry. A numerical example is presented to illustrate the application of the method developed.

This analytical investigation covers a range of coolant flows, corrugation amplitude varying from 0.030 to 0.300 inch, corrugation thickness varying from 0.0050 to 0.015 inch, and corrugation spacing varying from 0.020 to 0.050 inch. Both laminar and turbulent flow were considered with the transition region between Reynolds numbers of 2000 and 8000 in accordance with reference 4.

ANALYSIS

Equations are derived that form the basis for the construction of charts relating the corrugation geometry and coolant flow to the effective inside heat-transfer coefficient. In addition, a procedure is developed for evaluating the required effective inside heat-transfer coefficient for any specific application of air-cooled turbine blades. The coolant-flow requirements can be determined for each corrugation geometry by utilizing the charts in conjunction with a curve of the required effective inside heat-transfer coefficient. Also, curves are presented so that

the friction coefficient and thus the pressure requirements can be obtained for each corrugation geometry and coolant flow. The corrugation geometry requiring the minimum coolant flow can then be selected on the basis of the pressure available and the ease of fabrication. Finally, equations and curves are presented for determining the absolute minimum coolant flow irrespective of pressure drop.

Since the purpose of this report is to present a method of design of corrugated surfaces for application to air-cooled turbine blades, the type of blade shown in figure 1(a) is considered herein. This blade, which has an island insert, permits corrugations of uniform height and thus a more uniform peripheral distribution of coolant flow. Because of the island insert, the design method presented herein is restricted to corrugated sections having heat input on one side only.

A typical corrugated section of an air-cooled corrugated blade with an island insert (fig. 1(a)) such that heat is transferred to only one side of the corrugated section is shown in figure 1(b). The principal dimensions of the corrugation are the corrugation thickness τ, the corrugation amplitude Y, and the spacing or distance between fins m, where $m+\tau$ is the conventional center-to-center distance (see fig. 1(b)). (The symbols used in this report are listed in appendix A.) Since it is difficult to write such equations as for flow area and wetted perimeters for a typical corrugation as shown in figure 1(b), the typical corrugation has been idealized in the form of a rectangular corrugation as shown in figure 1(c). It is of interest to show the resultant equivalent fin (fig. 1(d)), where L is the equivalent fin length. Equations of the corrugation geometry may now be written for a section of the idealized corrugation, and the equations may be adapted to a section of the typical corrugation. Corrections required to adapt the idealized corrugation to the typical corrugation were at most 3.5 percent. A small braze fillet was assumed to bond the typical corrugation to the blade shell and island insert. (The equations of corrugation geometry are given in appendix B. The assumptions used in this analysis are listed in appendix C.)

Convective Heat-Transfer Coefficients

Recent experimental heat-transfer investigations for air flowing in both corrugated shapes (refs. 3 and 4) and noncircular ducts (ref. 5) have shown that round-tube correlations may be employed in the turbulent region. Reference 4 shows that for air flowing through corrugated shapes in the laminar region, the Nusselt number is a function of the rectangular tube aspect ratio α. In addition, the investigations of reference 5, which cover wall-to-air temperature differences up to 1200° F, suggest that the fluid properties be based on film temperature (arithmetic average of the surface and bulk temperatures) wherein the fluid

thermal conductivity varies as the square root of the temperature. For these reasons, the present analysis used conventional round-tube correlations for the turbulent region, the results of reference 4 for the laminar region, and fluid properties defined as in reference 5. For simplicity, fully developed flow was assumed, assuring conservative inside heat-transfer coefficients.

No analytical information is presently available for flow in the transition region. However, reference 4 presents experimental results for air flowing through corrugated shapes of different aspect ratio in the laminar, turbulent, and transition flow regions. The data indicate that the heat-transfer results may be represented by a smooth curve in the transition region over a range of Reynolds number from 2000 to 8000. The results presented in reference 4 are therefore used in the present analysis to establish the transition region.

The heat-transfer correlations used to obtain the convective inside heat-transfer coefficients for the laminar, transition, and turbulent flow regions are shown in figure 2. For laminar flow, the results on figure 2 are expressed by the equation

$$Nu = F(\alpha) \tag{1}$$

or

$$\frac{Nu}{Re} = \frac{F(\alpha)}{Re} \tag{2}$$

where $F(\alpha)$ is given in reference 4. The line representing turbulent flow was obtained utilizing the following equation (ref. 5):

$$Nu = 0.023\ (Re)^{0.8}\ (Pr)^{0.4} \tag{3}$$

Since the Prandtl number varies only slightly with temperature and has a constant value of 0.655 for temperatures above approximately 1000° F (ref. 6), its effect on heat-transfer correlations is negligible. Therefore, with Pr assumed equal to 0.655, equation (3) becomes

$$\frac{Nu}{Re} = \frac{0.019}{(Re)^{0.2}} \tag{4}$$

The correlations representing the heat transfer in the transition region were established by following the experimental trends shown in reference 4.

In accordance with reference 5, the thermal conductivity of the air is directly proportional to the square root of the temperature. In

addition, the viscosity of the air may be approximated by $\mu_a \propto T^{0.7}$. With a reference temperature of 1000° R used to evaluate the constants of proportionality, the expressions for the thermal conductivity and viscosity become, respectively,

$$\frac{k_{a,f}}{k_{a,1000}} = \left(\frac{T_f}{1000}\right)^{0.5} \tag{5}$$

and

$$\frac{\mu_{a,f}}{\mu_{a,1000}} = \left(\frac{T_f}{1000}\right)^{0.7} \tag{6}$$

Equation (5) is used to express the Nusselt number as

$$Nu = \frac{h_a D_h}{k_{a,1000}\left(\frac{T_f}{1000}\right)^{0.5}} \tag{7}$$

Similarly, equation (6) is used to give the Reynolds number as

$$Re = \frac{w D_h \left(\frac{T_b}{T_f}\right)}{gA_f \mu_{a,1000}\left(\frac{T_f}{1000}\right)^{0.7}} \tag{8}$$

Employing the coolant flow per inch of corrugation $w/(m+\tau)$ in equation (8) gives

$$Re = \left(\frac{w}{m+\tau}\right)\left(\frac{1000}{T_f}\right)^{0.7}\left(\frac{T_b}{T_f}\right)\frac{(m+\tau) D_h}{gA_f \mu_{a,1000}} \tag{9}$$

Effective Inside Heat-Transfer Coefficient

The effective inside heat-transfer coefficient is used for evaluating the coolant-flow requirements since it is an over-all coefficient based on the blade shell temperature and the blade shell surface area.

Equation (6) of reference 7 presents the following relation for the effective heat-transfer coefficient for a coolant passage containing augmented heat-transfer surfaces such as fins or corrugations:

$$h_f = \frac{h_a}{m+\tau}\left[\frac{2\tanh\left(\frac{2h_a}{K\tau}\right)^{0.5} L}{\left(\frac{2h_a}{K\tau}\right)^{0.5}} + m\right] \tag{10}$$

wherein consistant units are employed. Expressing h_a in terms of the Nusselt number as given by equation (7) results in

$$h_f = \frac{(Nu)(k_{a,1000})\left(\frac{T_f}{1000}\right)^{0.5}}{D_h\,(m+\tau)}\left\{\frac{2\tanh\left[\frac{2(Nu)(k_{a,1000})\left(\frac{T_f}{1000}\right)^{0.5}}{K\tau\,D_h}\right]^{0.5} L}{\left[\frac{2(Nu)(k_{a,1000})\left(\frac{T_f}{1000}\right)^{0.5}}{K\tau\,D_h}\right]^{0.5}} + m\right\} \tag{11}$$

The effective inside heat-transfer coefficient h_f for laminar, transition, or turbulent flow is given by equation (11) once the corresponding Nusselt number is incorporated. For the purpose of constructing the charts, equation (11) is rewritten employing a base value of thermal conductivity of 16 Btu per hour per foot per $^{\circ}F$ (this value is typical for high-temperature alloys).

$$h_f\left(\frac{1000}{T_f}\right)^{0.5} = \frac{(Nu)(k_{a,1000})}{D_h\,(m+\tau)}\left\{\frac{2\tanh\left[\frac{2(Nu)(k_{a,1000})}{16\tau\,D_h}\right]^{0.5}\left[\left(\frac{16}{K}\right)\left(\frac{T_f}{1000}\right)^{0.5}\right]^{0.5} L}{\left[\frac{2(Nu)(k_{a,1000})}{16\tau\,D_h}\right]^{0.5}\left[\left(\frac{16}{K}\right)\left(\frac{T_f}{1000}\right)^{0.5}\right]^{0.5}} + m\right\} \tag{12}$$

Charts

Plots of the heat-transfer parameter $h_f\,(1000/T_f)^{0.5}$ against the coolant-flow parameter $\frac{w}{m+\tau}\left(\frac{1000}{T_f}\right)^{0.7}\frac{T_b}{T_f}$ are obtained using the relation given by equation (12). The Nusselt number of equation (12) is obtained from figure 2 for each value of $\frac{w}{m+\tau}\left(\frac{1000}{T_f}\right)^{0.7}\frac{T_b}{T_f}$ using equation (9) to evaluate the Reynolds number. Three values of the parameter $(16/K)(T_f/1000)^{0.5}$ contained in equation (12) were assigned where K and T_f have the units of Btu per hour per foot per $^{\circ}F$ and $^{\circ}R$, respectively. The range covered by these three values was considered adequate for most applications. The plots relating the heat-transfer parameter to the coolant-flow parameter are presented in the form of working charts. Charts I, II, and III are for values of the parameter $(16/K)(T_f/1000)^{0.5}$ equal to 0.5, 1.0, and 2.0, respectively. Each chart consists of nine figures covering a range of corrugation amplitudes from 0.030 to 0.30 inch; corrugation spacings of 0.020, 0.035, and 0.050 inch; and corrugation thicknesses of 0.005, 0.010, and 0.015 inch. Each figure is plotted for the range of amplitudes and one value each of spacing and thickness and covers the laminar, transition, and turbulent flow regions. The transition region, which extends from a Reynolds number of 2000 to 8000, is represented by dashed lines on the charts.

The maximum difference in the heat-transfer parameter between charts I and II or charts II and III due to the differences in the parameter $(16/K)(T_f/1000)^{0.5}$ ranges from approximately 35 percent for $Y = 0.30$ inch to 8 percent for $Y = 0.030$ inch. Although interpolations may be employed for intermediate values of $(16/K)(T_f/1000)^{0.5}$, it is sufficiently accurate for most engineering purposes to use the chart with the value of $(16/K)(T_f/1000)^{0.5}$ nearest the value for the conditions being considered.

Friction Coefficients

Figure 3 presents curves from which the friction coefficient can be obtained in order to evaluate the pressure drop through corrugated passages. As in the case of the heat-transfer correlations, the friction coefficients for the laminar region were obtained from reference 4. In

addition, the friction coefficients in the turbulent region are represented by the Kármán-Nikuradse line. This line was shown to correlate the large amount of data in reference 5. The transition region on figure 3 was established from the experimental results of reference 4.

In accordance with the results of reference 5, the fluid properties are based on film temperature. Therefore, the friction coefficient is defined by (eq. (16) of ref. 5)

$$f_f = \frac{\left(\frac{\Delta F_d}{A_f}\right)}{4\frac{\Delta x}{D}\ \frac{\rho_f W^2}{2}} \tag{13}$$

and the Reynolds number, by equation (9).

Required Effective Heat-Transfer Coefficient

A coolant passage having fins or corrugations has for its particular material and operating conditions a specified maximum allowable surface temperature distribution. The average chordwise allowable blade temperature of an air-cooled turbine blade varies inversely with the blade stresses. The effective inside heat-transfer coefficient specified by the maximum allowable blade temperature at a particular span position is herein designated the required effective heat-transfer coefficient $h_{f,req}$. This coefficient varies along the blade span and is a function of the coolant flow. The procedure for determining $h_{f,req}$ is discussed in the following paragraphs.

The equation for the one-dimensional temperature distribution of an air-cooled turbine blade with heat transfer and rotation is (see appendix D)

$$\varphi + \Phi = \frac{1}{1+\lambda}\, e^{-\left[\frac{1}{1+\lambda}\ \frac{h_o x}{c_p\left(\frac{w}{m+\tau}\right)12}\right]} \tag{14}$$

where

$$\varphi \equiv \frac{T_{g,e} - T_B}{T_{g,e} - T''_{a,in}}$$

$$\Phi \equiv \frac{\omega^2 \left(\frac{w}{m+\tau}\right) 12\, x}{gJh_o(T_{g,e} - T''_{a,in})} \left\{1 - e^{-\left[\frac{1}{1+\lambda} \frac{h_o x}{c_p \left(\frac{w}{m+\tau}\right) 12}\right]}\right\}$$

$$\left[\frac{\omega^2 \left(\frac{w}{m+\tau}\right) 12}{gJh_o(T_{g,e} - T''_{a,in})}\right] \left[\frac{c_p \left(\frac{w}{m+\tau}\right) 12(1+\lambda)}{h_o} - r_{in}\right] \tag{15}$$

$$\lambda \equiv \frac{h_o}{h_f}$$

Equation (14) applies to stationary turbine blades if the rotational terms are omitted ($\omega = 0$). Once the allowable blade temperature at any spanwise position is fixed and all operating conditions are specified, equation (14) implicitly expresses the value of λ_{req} and therefore the required effective heat-transfer coefficient $h_{f,req}$ as a function of the coolant flow. Since this involves a lengthy trial-and-error solution, equation (14) is modified in appendix D such that an approximate solution is obtained directly. A first-order approximation for the rotational effects yields the equation

$$\Phi \approx \Phi_{app} \equiv \varphi \left\{ \frac{T_{g,e} - T''_{a,in}}{T_{g,e} - \left[T''_{a,in} + \frac{\omega^2 x}{2gJc_p}(x + 2r_{in})\right]} - 1 \right\} \tag{16}$$

where Φ_{app} is independent of both $w/(m+\tau)$ and λ. If Φ of equation (14) is approximated by equation (16), equation (14) can be solved, without iteration, to determine the variation of $h_{f,req}$ with $w/(m+\tau)$

at any spanwise position once the allowable blade temperature is fixed and all operating conditions are specified. The right side of equation (14) has been plotted in figure 4 to permit this direct solution. In addition, the ratio Φ_{app}/Φ has been computed in appendix D and is plotted in figure 5 against $\frac{1}{1+\lambda}\frac{h_o x}{c_p\left(\frac{w}{m+\tau}\right)12}$. The value of this ratio can now be used to obtain a second-order correction for the rotational effects by using the approximate value of $\frac{1}{1+\lambda}\frac{h_o x}{c_p\left(\frac{w}{m+\tau}\right)12}$ as determined with Φ_{app} as the first-order correction. A comparison of the solutions of λ_{req} for severe conditions obtained using both the exact and approximate methods is presented in appendix D. This comparison shows excellent agreement between the exact solution and the approximate solution with second-order correction.

For any allowable turbine blade temperature distribution and specified operating conditions (methods for obtaining $T_{B,al}$ and h_o will be discussed in the numerical example), curves of $h_{f,req}$ against $w/(m+\tau)$ can be plotted for various spanwise positions. Such a set of curves is illustrated in figure 6(a). The upper envelope curve represents the minimum values of the effective heat-transfer coefficients that will provide adequate cooling at all spanwise positions. The spanwise position critical for a given coolant flow is that at which the $h_{f,req}$ curve is tangent to the envelope curve (see fig. 6(a)). By definition, the critical section of an air-cooled blade is the spanwise position where a curve of the actual blade temperature distribution obtained for a given coolant flow is tangent to a curve of the spanwise allowable blade temperature distribution (ref. 1).

Once the envelope curve of $h_{f,req}$ has been determined for a specific application, it is transformed to the scale and ordinate and abscissa of charts I, II, and III. Figure 6(b) presents the transformed envelope curve of figure 6(a). The transformed $h_{f,req}$ curve can now be superimposed on the working charts for evaluating the required coolant flow for each corrugation geometry. With this value of required coolant flow, the corresponding pressure requirements can be computed.

Absolute Minimum Coolant Flow

In some instances, it may be desirable to determine the minimum coolant flow required irrespective of blade configuration or pressure requirements in order to evaluate potential improvements in the design of corrugated blades. In addition, the minimum coolant flow may be used to estimate quickly the coolant requirements for any specific application. An envelope curve of $h_{f,req}$ such as shown in figure 6(a) approaches the minimum value of coolant flow asymptotically. This value of coolant flow is herein called the absolute minimum coolant flow, and for a particular set of design conditions is limited by the heat capacity of the coolant. The value of the absolute minimum coolant flow can be determined from figure 4, which covers the complete range of effective heat-transfer coefficients from zero to infinity. For a given value of the ordinate, $\varphi_{req} + \Phi$, wherein φ is replaced by φ_{req}, a maximum value of $\frac{h_o x}{c_p\left(\frac{w}{m+\tau}\right)12}$ can be obtained. From this value of $\frac{h_o x}{c_p\left(\frac{w}{m+\tau}\right)12}$, the absolute minimum coolant flow for any value of $h_o x$ can be determined. Values of these absolute minimum coolant flows for a range of values of $\varphi_{req} + \Phi$ have been determined from figure 4 and are plotted against $h_o x$ in figure 7. For values of $\varphi_{req} + \Phi > 0.368$, the effective heat-transfer coefficients required for the minimum coolant flows are infinite.

Figure 7 can be used for determining the absolute minimum coolant flow if the values of $h_o x$ and $\varphi_{req} + \Phi$ are specified. Both $h_o x$ and φ_{req} can be readily specified at any spanwise position from the particular design conditions. However, Φ is interrelated with the coolant flow and the effective heat-transfer coefficient. It is therefore advantageous to express $\varphi_{req} + \Phi$ as follows:

$$\varphi_{req} + \Phi = \varphi_{req} + \frac{\Phi_{app}}{\Phi_{app}/\Phi}$$

or

$$\varphi_{req} + \Phi = \varphi_{req}\left(1 + \frac{\Phi_{app}/\varphi_{req}}{\Phi_{app}/\Phi}\right) \tag{17}$$

Now Φ_{app}/φ_{req} is independent of the coolant flow or effective heat-transfer coefficient and can be computed from equation (16). In

addition, Φ_{app}/Φ is related only to $\varphi_{req} + \Phi$ for the conditions corresponding to the absolute minimum coolant flow. This may be understood by recalling that for these conditions any value of $\varphi_{req} + \Phi$ specifies both $\frac{h_o x}{c_p\left(\frac{w}{m+\tau}\right)12}$ and $1/1+\lambda$ (fig. 4). Therefore, since figure 5 relates Φ_{app}/Φ to the product of $1/1+\lambda$ and $\frac{h_o x}{c_p\left(\frac{w}{m+\tau}\right)12}$, a knowledge of $\varphi_{req} + \Phi$ is sufficient for determining Φ_{app}/Φ. Consequently, equation (17) has been plotted in figure 8. From the particular design conditions and any value of x/b, values of φ_{req}, Φ_{app}/Φ_{req}, and $h_o x$ can now be computed. With these values, $\varphi_{req} + \Phi$ can be read from figure 8 and, then, the absolute minimum coolant flow can be read from figure 7. Several values of x/b and the corresponding value of φ_{req} must be considered in order to determine the maximum value of the absolute minimum coolant flow.

PROCEDURES AND USE OF CHARTS AS ILLUSTRATED BY A NUMERICAL EXAMPLE

The procedure and charts contained in this report have been set up for the purpose of furnishing a corrugation geometry which gives for a specific application the best combination of (1) high heat-transfer effectiveness and (2) lowest possible coolant flow within pressure-drop limitations. The application chosen for the numerical example is the selection of a corrugation geometry for an air-cooled turbine rotor blade.

Before the procedures and charts can be used, certain independent variables must be known or calculated. These variables are determined from the operating conditions of the engine being considered, and they remain fixed in the selection of the best corrugation geometry. For this example, an engine was chosen from reference 8 as one representative of futuristic air-cooled turbojet engines with a turbine inlet temperature of 3000° R. The data required are as follows:

(a) Average effective gas temperature $T_{g,e}$, 2653° R

(b) Relative total cooling-air temperature at turbine blade inlet $T''_{a,in}$, 1013° R

(c) Relative total cooling-air pressure at turbine blade inlet $p''_{a,in}$, 5120 pounds per square foot

(d) Average static gas pressure across turbine rotor tip p_g, 5416 pounds per square foot

(e) Turbine hub-tip radius ratio r_T/r_{in}, 0.70

(f) Turbine hub radius r_{in}, 1.05 feet

(g) Turbine blade span b, 0.45 foot

(h) Turbine tip speed U_T, 1700 feet per second

(i) Angular velocity ω, 1133 radians per second

(j) Average outside heat-transfer coefficient h_o as calculated by the method presented in reference 9, 0.0642 Btu per second per square foot per ^oF

Evaluation of Required Effective Heat-Transfer Coefficient

If curves of $h_{f,req}$ against coolant flow are to be plotted for various spanwise positions x/b, the maximum allowable blade temperature $T_{B,al}$ must be known at these positions. Values of $T_{B,al}$ are based on the local spanwise blade stress level, the stress-to-rupture properties of the blade material, and a suitable factor of safety or stress-ratio factor (ref. 1). A limited amount of experimental information is available (ref. 10) on stress-ratio factors for a particular air-cooled blade configuration and blade material.

Blade spanwise positions x/b equal to 0, 0.25, 0.50, 0.65, 0.75, and 0.90 were selected for this example. The blade taper ratio (defined as the ratio of the blade metal area at the tip to the blade metal area at the root) was taken as 0.60, and the blade stress level was calculated by means of figure 2 in reference 11. The values of design stresses S (defined as blade centrifugal stress multiplied by a stress-ratio factor) and the maximum allowable blade temperature $T_{B,al}$ are given in the following table for the selected values of x/b:

Spanwise position, x/b	Design stress S calculated using ref. 11 and a value of stress-ratio factor of 1.50, lb/sq in.	$T_{B,al}$ obtained from S and stress-to-rupture properties of blade material, ^oR
0	93,300	1569
.25	75,900	1643
.50	56,000	1730
.65	39,800	1797
.75	30,850	1849
.90	13,060	1967

The stress-to-rupture properties in this table are obtainable from recently developed high-temperature alloys.

A setup and calculation typical of those required for determining $h_{f,req}$ against $w/(m+\tau)$ for $x/b = 0.25$ are as follows:

(1) From the values of $T_{g,e}$, $T''_{a,in}$, and $T_{B,al}$,

$$\varphi_{req} = \frac{T_{g,e} - T_{B,al}}{T_{g,e} - T''_{a,in}} = \frac{2653 - 1643}{2653 - 1013} = 0.616$$

(2) Calculate Φ_{app} from equation (16)

$$\Phi_{app} \equiv \varphi \left\{ \frac{T_{g,e} - T''_{a,in}}{T_{g,e} - \left[T''_{a,in} + \frac{\omega^2 x}{2gJc_p} (x + 2r_{in}) \right]} - 1 \right\}$$

$$\Phi_{app} = 0.616\ (0.016) = 0.00986$$

and thus,

$$\varphi_{req} + \Phi_{app} = 0.6258$$

(3) The parameter $\dfrac{h_o x}{c_p \left(\frac{w}{m+\tau}\right) 12}$ is determined by assuming values of $w/(m+\tau)$. (Interpolation in the case of figure 4 may be eliminated by assuming even values of the parameter $\dfrac{h_o x}{c_p \left(\frac{w}{m+\tau}\right) 12}$ and calculating the corresponding $w/(m+\tau)$.) Assuming $c_p = 0.24$ Btu per pound per ^{o}F gives

$$\frac{h_o x}{c_p\ 12} = 0.00251$$

(4) The following setup is now recommended for obtaining $h_{f,req}$ at the desired x/b position, which is 0.25 in this case:

1	2	3	4	5	6	7	8	9	10
Assume $\frac{w}{m+\tau}$	$\frac{h_o x}{c_p\left(\frac{w}{m+\tau}\right)12}$	$\frac{1}{1+\lambda}$, $\varphi_{req} + \Phi_{app}$, ②, fig. 4	②×③	$\frac{\Phi_{app}}{\Phi}$, ④, fig. 5	Φ, $\frac{\Phi_{app}}{⑤}$	$\varphi_{req} + \Phi$	$\frac{1}{1+\lambda_{req}}$, ②, ⑦, fig. 4	λ_{req}	$h_{f,req}$, $\frac{h_o}{⑨}$
0.012	0.209	0.730	0.1525	0.926	0.01065	0.6266	0.731	0.369	0.1740
.016	.157	.698	.1095	.947	.0104	.6264	.695	.440	.1458
.020	.1255	.680	.0852	.958	.0103	.6263	.690	.470	.1365
.024	.1046	.670	.0701	.965	.0102	.6263	.670	.493	.1302
.030	.0837	.660	.0552	.972	.01015	.6261	.660	.515	.1246

(5) Plot $h_{f,req}$ against $w/(m+\tau)$ at each x/b position and determine the upper envelope (see fig. 6(a)).

Evaluation of Cooling-Air Temperature at Blade Outlet, Cooling-Air Bulk Temperature, and Film Temperature

The cooling-air temperature at the blade outlet $T''_{a,out}$ can be determined from a heat balance once the actual blade temperature at the blade outlet $T_{B,out}$ is computed using equation (14). The heat balance required for determining $T''_{a,out}$ is

$$h_o(T_{g,e} - T_{B,out}) = h_{f,req}(T_{B,out} - T''_{a,out}) \tag{18}$$

Once $T''_{a,out}$ is known for a number of coolant flows $w/(m+\tau)$, the average cooling-air bulk temperature T_b can be evaluated from the following equation for any value of $w/(m+\tau)$:

$$T_b = \frac{T''_{a,in} + T''_{a,out}}{2} \tag{19}$$

An average blade temperature $T_{B,av}$ must be obtained in order to determine the average film temperature T_f. It is convenient and sufficiently accurate to obtain $T_{B,av}$ from the following heat balance:

$$h_o(T_{g,e} - T_{B,av}) = h_{f,req}(T_{B,av} - T_b) \tag{20}$$

Then T_f is evaluated from

$$T_f = \frac{T_b + T_{B,av}}{2} \tag{21}$$

A calculation typical of that required to determine $T''_{a,out}$, T_b, and T_f is presented for one value of coolant flow $w/(m+\tau) = 0.020$ pound per second per inch. It is suggested that a sufficient number of coolant flows be used that a curve of $T''_{a,out}$ against $w/(m+\tau)$ and thus curves of T_b and T_f against $w/(m+\tau)$ can be obtained.

(1) First it is necessary to determine $T_{B,out}$. This will be done by utilizing equation (14) and figures 4 and 5. For $w/(m+\tau) = 0.020$ pound per second per inch, $h_{f,req} = 0.143$ Btu per second per foot per ^{o}F from the envelope curve of figure 6(a). The following parameters must now be calculated:

$$\frac{h_o b}{c_p\left(\frac{w}{m+\tau}\right)12} = \frac{(0.0642)(0.450)}{(0.124)(0.020)(12)} = 0.502$$

$$\frac{1}{1+\lambda_{req}} = \frac{1}{1 + \frac{0.0642}{0.143}} = 0.690$$

$$\frac{1}{1+\lambda_{req}} \cdot \frac{h_o b}{c_p\left(\frac{w}{m+\tau}\right)12} = 0.346$$

From figure 4,

$$\varphi + \Phi = 0.486$$

or

$$\varphi + \Phi_{app} \Big/ \left(\frac{\Phi_{app}}{\Phi}\right) = 0.486$$

The value of Φ_{app}/Φ is obtained from figure 5,

$$\frac{\Phi_{app}}{\Phi} = 0.838$$

and Φ_{app} is evaluated from equation (16) as

$$\Phi_{app} = 0.08\varphi$$

Thus,

$$\varphi + \Phi_{app} \Big/ \left(\frac{\Phi_{app}}{\Phi}\right) = \varphi + \frac{0.08\varphi}{0.838} = 0.486$$

and

$$\varphi = 0.444$$

From the definition of φ, $T_{B,out}$ may be determined.

$$T_{B,out} = T_{g,e} - \varphi(T_{g,e} - T''_{a,in})$$

$$T_{B,out} = 2653 - 0.444\ (2653 - 1013) = 1925^{\circ}\ R$$

(2) Equation (18) is now used to evaluate $T''_{a,out}$.

$$T''_{a,out} = T_{B,out} - \frac{h_o}{h_{f,req}} (T_{g,e} - T_{B,out})$$

$$T''_{a,out} = 1925 - \frac{0.0642}{0.143} (2653 - 1925) = 1598^{\circ}\ R$$

(3) From equation (19),

$$T_b = \frac{1013 + 1598}{2} = 1305^{\circ}\ R$$

(4) The average film temperature T_f is determined by first obtaining $T_{B,av}$ from equation (20).

$$T_{B,av} = \frac{T_{g,e} + \frac{h_{f,req}}{h_o}(T_b)}{\left(1 + \frac{h_{f,req}}{h_o}\right)}$$

$$T_{B,av} = \frac{2653 + \frac{0.143}{0.0642}(1305)}{\left(1 + \frac{0.143}{0.0642}\right)} = 1724^\circ \text{ R}$$

Thus, from equation (21),

$$T_f = \frac{1305 + 1724}{2} = 1514^\circ \text{ R}$$

Use of Charts to Obtain Coolant Flow

The designer now has a choice of charts I, II, or III. For this example, the blade material is assumed to have a thermal conductivity of K = 20 Btu per hour per foot per $^\circ$F. This value of K was considered to remain constant. Since the variation of film temperature with coolant flow is small, an average value of $T_f = 1510^\circ$ R was used. Thus, the parameter $(16/K)(T_f/1000)^{0.5}$ becomes 0.982, and chart II for $(16/K)(T_f/1000)^{0.5} = 1.0$ is used for this example.

The envelope curve of $h_{f,req}$ (fig. 6(a)) as converted to the variables of the ordinate and abscissa of chart II is shown on figure 6(b). This conversion was made utilizing the variation in T_b and T_f with $w/(m+\tau)$. In order to determine the coolant-flow requirements for each combination of the geometric parameters Y, m, and τ, the $h_{f,req}$ curve was drawn on vellum paper and then superimposed on each figure of chart II. Values of the coolant-flow parameter $\frac{w}{m+\tau}\left(\frac{1000}{T_f}\right)^{0.7}\frac{T_b}{T_f}$ were read

and tabulated for each combination of Y, m, and τ considered. Values of Y greater than 0.15 were eliminated in this example since they were considered impractical for conventional turbine blade sizes.

Once the values of $\frac{w}{m+\tau}\left(\frac{1000}{T_f}\right)^{0.7}\frac{T_b}{T_f}$ corresponding to the intersection of the $h_{f,req}$ curve and the curves for each Y considered are tabulated, the actual coolant flow $w/(m+\tau)$ must be determined. For this purpose, it is suggested that a supplementary curve of $\frac{w}{m+\tau}\left(\frac{1000}{T_f}\right)^{0.7}\frac{T_b}{T_f}$ against $w/(m+\tau)$ be obtained. Such a curve is easily obtained from the curves of T_b and T_f against $w/(m+\tau)$ determined previously.

Calculation of Pressure Change

The charts presented in reference 12 are used to determine the pressure change for this required coolant flow for each corrugation geometry considered in the preceding section. As an illustration of the procedures of reference 12, the pressure change will be obtained for the geometry combination $m = 0.20$, $\tau = 0.010$, and $Y = 0.10$.

(1) From the intersection of the $h_{f,req}$ curve and the curve for $Y = 0.10$ on chart II, $\frac{w}{m+\tau}\left(\frac{1000}{T_f}\right)^{0.7}\frac{T_b}{T_f} = 0.0112$ pound per second per inch. Then, use of the supplementary curve of $\frac{w}{m+\tau}\left(\frac{1000}{T_f}\right)^{0.7}\frac{T_b}{T_f}$ against $w/(m+\tau)$ results in the actual coolant flow $w/(m+\tau) = 0.01685$ pound per second per inch.

(2) In order to evaluate the parameter $w\sqrt{T''_{a,in}}/A_f\,p''_{a,in}$ of reference 12, the flow area is determined from the equation in appendix B, $A_f/m+\tau = 4.31\times10^{-4}$ square feet per inch. Thus,

$$\frac{w\sqrt{T''_{a,in}}}{A_f\,p''_{a,in}} = \frac{\left(\frac{w}{m+\tau}\right)\sqrt{T''_{a,in}}}{\left(\frac{A_f}{m+\tau}\right)p''_{a,in}} = \frac{(0.01685)\sqrt{1013}}{(4.31\times10^{-4})(5120)} = 0.243$$

(3) The friction parameter $4f_b/D_h$ contained in reference 12 (in terms of the symbols of ref. 12 this parameter is $4f/D_h$) is evaluated by determining the Reynolds number from equation (9) and thus the friction coefficient f_f from figure 3. From the definition of D_h, equation (9), and appendix B,

$$D_h = 0.00285 \text{ feet}$$

$$Re = 3820$$

$$\alpha = 4.50$$

Thus, from figure 3,

$$f_f = 0.0078$$

Now, since the friction coefficient is inversely proportional to density or directly proportional to temperature (see eq. (13)), f_b can be obtained from

$$f_b = \left(\frac{T_b}{T_f}\right) f_f$$

$$f_b = \left(\frac{1352}{1528}\right)(0.0078) = 0.0069$$

Thus, the friction parameter becomes

$$\frac{4f_b}{D_h} = 9.68$$

(4) The blade inlet Mach number M_{in} is obtained from figure 1 of reference 12 using the parameter $w\sqrt{T''_{a,in}}/A_f\, p''_{a,in}$

$$M_{in} = 0.277$$

(5) Using a linear variation of cooling-air temperature through the blade and the incremental distance Δx of reference 12 as $b/2$ gives the blade outlet Mach number M_{out} as

$$M_{out} = 0.379$$

(6) Once M_{out} is known, figure 1 of reference 12 is used to determine the blade outlet total or static pressure.

In some cases, for a particular corrugation geometry, choking may occur in the blade and the required coolant flow cannot be passed. This geometry configuration would therefore be unsatisfactory.

Reduction of Data and Selection of Coolant Passage Configuration

As the required coolant flow decreases for given values of m and τ, the pressure drop through the corrugation configuration increases corresponding to decreasing values of Y. In addition, the coolant Mach numbers at the blade inlet and outlet may increase to the point of choking. When either choking occurs or the pressure drop is equal to the pressure drop available, the minimum coolant flow for the given m and τ is determined. This in turn determines the value of Y for the minimum value of coolant flow. For this reason, it is suggested that the calculated pressure drops for the various values of Y at fixed m and τ be used to determine the value of Y corresponding to the condition of calculated pressure drop equal to available pressure drop. Thus, for each value of m and τ, a minimum coolant flow with its corresponding value of Y is determined. Although a further reduction of the data may be obtained from additional plots, the designer can, at this point, make a selection of the best corrugation geometry configuration by an inspection of the resulting data. The procedure of determining Y for the minimum coolant flow will be better illustrated in the following table for m = 0.020 inch and τ = 0.010 inch:

Y	Coolant flow, $\frac{w}{m+\tau}$	Static pressure at passage outlet	Gas static pressure across rotor tip
0.03	No solution, choking	----	5416
.05	No solution, choking	----	5416
.07	No solution, choking	----	5416
.10	0.01685	4540	5416
.15	.01806	5940	5416
.131	.0176	5416	5416

This table shows that for values of Y equal to 0.030, 0.050, and 0.070 inch, the passage was choked and thus no solution was obtained since the required coolant flow could not be passed. Solutions were obtained, however, at values of Y equal to 0.10 and 0.15 inch, and the corresponding static pressures at the passage outlet are tabulated along with the average gas static pressure across the rotor tip. If it is assumed that the required static pressure at the passage outlet is equal to the average gas static pressure, it is apparent that the minimum required coolant flow is obtained for a value of Y between 0.10 and 0.15 inch. From a linear interpolation of the static pressures at the passage outlet, the minimum required value of coolant flow is 0.0176 pound per second per inch for Y equal to 0.131 inch. It should be noted that $w/(m+\tau)$ is a true measure of the coolant flow since it is the air flow per inch of corrugation. In a similar manner, the minimum required coolant flow and Y were determined for all combinations of m and τ. These results are presented in table I for this example problem. For comparison, table I also includes the absolute minimum coolant flow obtained for the conditions of the example calculation. The procedure previously outlined was used to determine this absolute minimum coolant flow by considering a number of different span positions. This value occurred at a span position of $x/b = 0.75$. It is of interest that the absolute minimum coolant flow, which is independent of pressure drop, agrees within approximately 30 percent with the lowest required coolant shown in table I.

The corrugation geometry combinations presented in table I are all within pressure-drop limitations. Consequently, the best corrugation geometry for the application considered need be selected only on the basis of minimum coolant flow and ease of fabrication. Because of the size of present air-cooled turbine blades, a small value of Y is desirous. For example, even though the minimum coolant flow occurs for the geometry combination of $m = 0.020$, $\tau = 0.015$, and $Y = 0.143$, this configuration is rejected because of the large value of Y. With reference to table I, the corrugation geometry selected for the application being considered is $m = 0.020$, $\tau = 0.005$, and $Y = 0.10$ inch.

Another factor which should be considered in the final selection of a corrugation geometry is the weight of corrugation material because a reduction in blade weight results in a reduction in turbine weight and thus engine weight. Since the weight of corrugation material per running inch and per unit length is proportional to the cross-sectional area of the corrugation geometry (see appendix B), a comparison of weights can be made on an area basis. Thus, for a particular airfoil cross-sectional area, the increases or decreases in area due to the corrugation geometries must be compared for the various geometries considered in the final selection.

CONCLUDING REMARKS

A method utilizing charts has been devised for systematically determining an optimum corrugation geometry configuration for application to air-cooled turbine blades. These charts show that the cooling effectiveness varies appreciably with changes in geometry which may be reflected in improvements in the coolant flow and pressure requirements. For many engineering purposes, it may be sufficient and desirable to make a less detailed study than that suggested by the procedure presented in this report. For instance, in the example calculation the corrugation thickness τ, in general, had a relatively small effect upon the minimum coolant flow obtainable with the pressure drop available. The chief effect noticed in this example is that as the corrugation thickness τ is decreased, the amplitude Y is also decreased. Therefore, if small corrugation amplitudes are required (small corrugation amplitudes are desirable in order to provide trailing-edge cooling with minimum trailing-edge thickness), possibly only small values of thickness need be investigated. Similarly, the choice of the corrugation spacing m for initial calculations may be based on trends such as that indicated by the example calculation wherein the cooling requirements decrease with corrugation spacing. However, it should be realized that as the coolant flow changes from turbulent to laminar the trend obtained may also change. For instance, as the corrugation amplitude Y decreases, the available effective heat-transfer coefficient increases for turbulent flow, but generally decreases for laminar flow. For these reasons, no general trends can be established and reasonable care must be taken if only certain corrugation geometries are investigated. In any case, an inspection of the superimposition of the required effective heat-transfer coefficient curve on all figures of the chart being used seems advisable so that relative changes in weight flow requirements and flow conditions can be compared. Frequently, a quick estimation of the cooling requirements is desired without consideration of the coolant passage configuration. As shown by the example calculation, the absolute minimum coolant flow (irrespective of pressure drop limitations or geometric configurations), which can be readily computed without recourse to the working charts, is a reasonable indication of the coolant flow requirements.

For practical applications, an air-cooled blade with choked flow or the condition wherein the pressure drop is equal to the pressure drop available is undesirable. Such a design would provide no factor of safety. In addition, heat-transfer characteristics in the transition region and even Reynolds numbers for transition are somewhat uncertain. These factors should therefore be considered in the selection of a corrugation geometry configuration.

Lewis Flight Propulsion Laboratory
National Advisory Committee for Aeronautics
Cleveland, Ohio, August 30, 1954

APPENDIX A

SYMBOLS

The following symbols are used in this report:

A	cross-sectional metal area, sq in.
A_f	flow area, sq ft
b	blade length, or span, ft
c_p	specific heat at constant pressure, Btu/(lb)($^\circ$F)
D_h	hydraulic diameter, $4A_f/l_w$, ft
F	function
F_d	drag force, lb
f	friction coefficient
g	standard acceleration of gravity, ft/sec^2
h_a	convective inside heat-transfer coefficient for air, Btu/(sec)(sq ft)($^\circ$F)
h_f	effective inside heat-transfer coefficient, Btu/(sec)(sq ft)($^\circ$F)
$h_{f,req}$	required effective inside heat-transfer coefficient, Btu/(sec)(sq ft)($^\circ$F)
h_o	outside heat-transfer coefficient, Btu/(sec)(sq ft)($^\circ$F)
J	mechanical equivalent of heat, ft-lb/Btu
K	thermal conductivity of corrugation material
k_a	thermal conductivity of air, Btu/(sec)(ft)($^\circ$F)
$k_{a,1000}$	thermal conductivity of air at 1000° R, 7.2×10^{-6} Btu/(sec)(ft)($^\circ$F)
L	equivalent fin length, ft
l	perimeter, ft

M	Mach number relative to blade
m	fin spacing, ft unless specified in.
Nu	Nusselt number, $h_a D_h / k_a$
Pr	Prandtl number, $c_p \mu g / k_a$
p	static pressure, lb/sq ft abs
p"	total pressure with respect to rotating passage, lb/sq ft abs
Re	Reynolds number, $\rho W D_h / \mu g$
r	radius, ft
S	design stress, lb/sq in.
T	temperature, $^{\circ}R$
T"	total temperature with respect to rotating passage, $^{\circ}R$
U	blade speed, ft/sec
W	relative bulk velocity, ft/sec
w	coolant flow per corrugation, lb/sec
x	spanwise distance from blade inlet to any point on blade, ft
Y	corrugation amplitude, ft unless specified in.
α	aspect ratio, $\frac{\text{longer side of rectangular tube}}{\text{shorter side of rectangular tube}}$
λ	h_o / h_f
λ_{req}	$h_o / h_{f,req}$
μ	viscosity of air, slugs/(sec)(ft)
$\mu_{a,1000}$	viscosity of air at 1000° R, 6.00×10^{-7} slugs/(sec)(ft)
ρ	density, lb/sq ft
τ	fin thickness, ft unless specified in.

Φ_{app} first-order rotational correction parameter, eq. (16)

Φ second-order rotational correction parameter, eq. (15)

φ $\dfrac{T_{g,e} - T_B}{T_{g,e} - T''_{a,in}}$

ω angular velocity, radians/sec

Subscripts:

a air

al allowable

app approximate

av average

B blade

b bulk

e effective

f denotes film except when used with A and h

g combustion gas

in inlet

out outlet

req required

T tip

w wetted

APPENDIX B

EQUATIONS OF CORRUGATION GEOMETRY

(1) Flow area per inch of corrugation

$$\frac{A_f}{m+\tau} = 1.034 \frac{m(Y-\tau)}{m+\tau}$$

(2) Wetted perimeter per inch of corrugation

$$\frac{l_w}{m+\tau} = 0.987 \left[\frac{2(m+Y-\tau)}{m+\tau}\right]$$

(3) Equivalent fin length (ref. 1)

$$L = \frac{l_w - m}{2}$$

(4) Corrugation metal cross-sectional area per inch of corrugation

$$\frac{A}{m+\tau} = Y - \frac{A_f}{m+\tau} + \tau$$

(5) Aspect ratio

$$\alpha = \frac{Y-\tau}{m} \text{ for } (Y-\tau) \geq m$$

$$\alpha = \frac{m}{Y-\tau} \text{ for } (Y-\tau) \leq m$$

APPENDIX C

ASSUMPTIONS

1. The corrugation geometry is constant peripherally and longitudinally.

2. The convective inside heat-transfer coefficient is an average value for fully developed flow.

3. The viscosity of the coolant is expressed by $\mu_a \alpha T^{0.7}$.

4. The conductivity of the coolant is expressed by $k_a \alpha T^{0.5}$.

5. The transition region extends over a Reynolds number range from 2000 to 8000.

6. The thermal conductivity of the corrugation material is constant for any given application.

7. The outside surface length of the blade shell is equal to the inside surface length.

8. The outside heat-transfer coefficient and effective gas temperature are constant peripherally and longitudinally.

APPENDIX D

DERIVATION OF EQUATION USED FOR EVALUATING REQUIRED EFFECTIVE HEAT-TRANSFER COEFFICIENT

The temperature difference equation for determining the actual blade temperature at any blade spanwise position x (eq. (18) of ref. 7) is, in the present notation,

$$\varphi \equiv \frac{T_{g,e} - T_B}{T_{g,e} - T''_{a,in}} = \frac{1}{1+\lambda} e^{-\left[\frac{1}{1+\lambda} \frac{h_o x}{c_p \left(\frac{w}{m+\tau}\right) 12}\right]} - \frac{\omega^2 \left(\frac{w}{m+\tau}\right) 12 \, x}{g J h_o (T_{g,e} - T''_{a,in})} +$$

$$\left\{1 - e^{-\left[\frac{1}{1+\lambda} \frac{h_o x}{c_p \left(\frac{w}{m+\tau}\right) 12}\right]}\right\} \left[\frac{\omega^2 \left(\frac{w}{m+\tau}\right) 12}{g J h_o (T_{g,e} - T''_{a,in})}\right] \left[\frac{c_p \left(\frac{w}{m+\tau}\right) 12 \, (1+\lambda)}{h_o} - r_{in}\right] \tag{D1}$$

where

$$\lambda = \frac{h_o}{h_f}$$

Equation (D1) includes the cooling-air temperature change due to heat transfer and rotation.

If the maximum allowable blade temperature $T_{B,al}$ is employed, equation (D1) expresses the value of λ_{req} and thus $h_{f,req}$ as a function of the coolant flow. Since equation (D1) cannot be solved for λ either explicitly or directly by graphical procedures, an approximate solution is used to account for the rotational terms contained in the equation.

As a first-order approximation of equation (D1), it is assumed that the pumping work done on the cooling air between the blade inlet and the x position is added initially to avoid the use of the last two terms of

equation (D1) when calculating λ_{req}. This is accomplished by increasing $T''_{a,in}$ by the pumping work. For a rotating passage the necessary increase in the relative total cooling-air temperature is

$$\Delta T''_{a,in} = \frac{U_x^2 - U_{in}^2}{2gJc_p} = \frac{\omega^2}{2gJc_p}\left[(r_{in} + x)^2 - r_{in}^2\right]$$

or

$$\Delta T''_{a,in} = \frac{\omega^2 x\,(x + 2r_{in})}{2gJc_p} \tag{D2}$$

Using equation (D2), the first-order approximation for equation (D1) becomes

$$\frac{T_{g,e} - T_B}{T_{g,e} - \left[T''_{a,in} + \frac{\omega^2 x}{2gJc_p}(x + 2r_{in})\right]} = \frac{1}{1+\lambda}\, e^{-\left[\frac{1}{1+\lambda}\,\frac{h_o x}{c_p\left(\frac{w}{m+\tau}\right)12}\right]} \tag{D3}$$

For convenience, equation (D3) is rewritten in the form

$$\varphi + \Phi_{app} = \frac{1}{1+\lambda}\, e^{-\left[\frac{1}{1+\lambda}\,\frac{h_o x}{c_p\left(\frac{w}{m+\tau}\right)12}\right]} \tag{D4}$$

where

$$\Phi_{app} \equiv \Phi\left\{\frac{T_{g,e} - T''_{a,in}}{T_{g,e} - \left[T''_{a,in} + \frac{\omega^2 x}{2gJc_p}(x + 2r_{in})\right]} - 1\right\} \tag{16}$$

Equation (D4) can be solved graphically for λ as a function of coolant flow for any position x once the corresponding value of the blade temperature $T_{B,x}$ is assigned.

The accuracy of equation (D4) can be evaluated by a direct comparison of equations (D1) and (D4). This comparison, in turn, will provide

a correction which can be applied to equation (D4) for a more accurate evaluation of λ. For this purpose, equation (D1) can be written in the form

$$\varphi + \Phi = \frac{1}{1+\lambda} e^{-\left[\frac{1}{1+\lambda} \frac{h_o x}{c_p\left(\frac{w}{m+\tau}\right)12}\right]} \tag{14}$$

where

$$\Phi \equiv \frac{\omega^2\left(\frac{w}{m+\tau}\right)12\ x}{gJh_o(T_{g,e} - T''_{a,in})} - \left\{1 - e^{-\left[\frac{1}{1+\lambda} \frac{h_o x}{c_p\left(\frac{w}{m+\tau}\right)12}\right]}\right\}\left[\frac{\omega^2\left(\frac{w}{m+\tau}\right)12}{gJh_o(T_{g,e} - T''_{a,in})}\right]\left[\frac{c_p\left(\frac{w}{m+\tau}\right)12\ (1+\lambda)}{h_o} - r_{in}\right] \tag{15}$$

The form of the exact equation (eq. (D1)) as given by equation (14) is identical with the form of the approximate equation as given by equation (D4). If Φ_{app} of equation (D4) agrees with Φ of equation (14), the first-order approximation used in obtaining equation (D4) introduces no error. In evaluating the actual error, it is convenient to determine the ratio of Φ_{app} to Φ. By eliminating the value of φ from the definition of Φ_{app}, equation (D4) and (16) are combined to give

$$\Phi_{app} = \left\{\frac{1}{1+\lambda} e^{-\left[\frac{1}{1+\lambda} \frac{h_o x}{c_p\left(\frac{w}{m+\tau}\right)12}\right]} - \Phi_{app}\right\}\left\{\frac{T_{g,e} - T''_{a,in}}{T_{g,e} - \left[T''_{a,in} + \frac{\omega^2 x}{2gJc_p}(x + 2r_{in})\right]} - 1\right\} \tag{D5}$$

which upon solving for Φ_{app} becomes

$$\Phi_{app} = \frac{\omega^2(x^2 + 2r_{in}\,x)}{2gJc_p(T_{g,e} - T''_{a,in})} \frac{1}{1+\lambda} e^{-\left[\frac{1}{1+\lambda} \frac{h_o x}{c_p\left(\frac{w}{m+\tau}\right)12}\right]} \tag{D6}$$

The value of Φ_{app}/Φ is evaluated from the ratio of equation (D6) to (15), which upon simplification becomes

$$\frac{\Phi_{app}}{\Phi} = \frac{\left[\frac{1}{1+\lambda} \frac{h_o x}{c_p\left(\frac{w}{m+\tau}\right)12}\right] e^{-\left[\frac{1}{1+\lambda} \frac{h_o x}{c_p\left(\frac{w}{m+\tau}\right)12}\right]} \left(\frac{x}{2r_{in}} + 1\right)}{\frac{x}{r_{in}} - \left\{1 - e^{-\left[\frac{1}{1+\lambda} \frac{h_o x}{c_p\left(\frac{w}{m+\tau}\right)12}\right]}\right\} \left[\frac{(1+\lambda)\ c_p\left(\frac{w}{m+\tau}\right)12}{h_o x} \cdot \frac{x}{r_{in}} - 1\right]} \tag{D7}$$

Equation (D7) is plotted in figure 5 with the ratio Φ_{app}/Φ as the ordinate and $\frac{1}{1+\lambda} \frac{h_o x}{c_p\left(\frac{w}{m+\tau}\right)12}$ as the abscissa. The effect of x_{in} is so small that for convenience it is considered negligible. Now, figure 5 can be used to provide a second-order correction for equation (D1). This second-order correction is applied by using figure 5 and the resulting values of $1/1+\lambda_{req}$ obtained from figure 4 after the first-order correction is made. Then, with the ratio Φ_{app}/Φ known, Φ may be determined, since Φ_{app} was obtained previously. Thus, $\varphi + \Phi$ and figure 4 may be used to obtain new values of $1/1+\lambda_{req}$.

A check on the accuracy of the procedure for determining λ_{req} and thus $h_{f,req}$ was made by (1) solving equation (D1) for λ_{req} by trial-and-error methods ($\lambda_{req} = 0.318$), (2) neglecting the last two terms of equation (D1) and solving the first term for λ_{req}, thus giving the case

wherein the rotational effects are neglected and only heat transfer from the blade is considered ($\lambda_{req} = 0.474$), (3) solving for λ_{req} by applying the first-order correction ($\lambda_{req} = 0.351$), and (4) solving for λ_{req} by applying the first- and second-order corrections ($\lambda_{req} = 0.324$). The conditions selected for this check were considered to be a severe test, and the results show excellent agreement between the exact solution and the approximate solution with the second-order correction.

REFERENCES

1. Ziemer, Robert R., and Slone, Henry O.: Analytical Procedures for Rapid Selection of Coolant Passage Configurations for Air-Cooled Turbine Rotor Blades and for Evaluation of Heat-Transfer, Strength, and Pressure-Loss Characteristics. NACA RM E52G18, 1952.

2. Bartoo, Edward R., and Clure, John L.: Experimental Investigation of Air-Cooled Turbine Blades in Turbojet Engine. XII - Cooling Effectiveness of a Blade with an Insert and with Fins Made of a Continuous Corrugated Sheet. NACA RM E52F24, 1952.

3. London, A. L., and Ferguson, C. K.: Gas Turbine Plant Regenerator Surfaces - Basic Heat Transfer and Flow Friction Data. Res. Memo. No. 2-46, Bur. Ships. Navy Dept., July 1, 1946. (Navships (250-338-3).)

4. Kays, W. M., and Clark, S. H.: A Summary of Basic Heat Transfer and Flow Friction Design Data for Plain Plate-Fin Heat Exchanger Surfaces. Tech. Rep. No. 17, Dept. Mech. Eng., Stanford Univ., Aug. 15, 1953. (Contract N6-ONR-251, Task Order 6, (NR-090-104 for Office Navel Res.).)

5. Pinkel, Benjamin: A Summary of NACA Research on Heat-Transfer and Friction for Air Flowing Through Tube with Large Temperature Difference. Trans. A.S.M.E., vol. 76, no. 2, Feb. 1954, p. 305.

6. Eckert, E. R. G.: Introduction to the Transfer of Heat and Mass. McGraw-Hill Book Co., Inc., 1950.

7. Livingood, John N. B., and Brown, W. Byron: Analysis of Spanwise Temperature Distribution in Three Types of Air-Cooled Turbine Blades. NACA Rep. 994, 1950. (Supersedes NACA RM's E7B11e and E7G30.)

8. Rossback, Richard J., Schramm, Wilson B., and Hubbartt, James E.: Analysis of Factors Affecting Selection and Design of Air-Cooled Single-Stage Turbines for Turbojet Engines. I - Turbine Performance and Engine Weight-Flow Capacity. NACA RM E54C22, 1954.

9. Brown, W. Byron, and Donoughe, Patrick L.: Extension of Boundary-Layer Heat-Transfer Theory to Cooled Turbine Blades. NACA RM E50F02, 1950.

10. Stepka, Francis S., Bear, Robert H., and Clure, John L.: Experimental Investigation of Air-Cooled Turbine Blades in Turbojet Engines. XIV - Endurance Evaluation of Shell-Supported Turbine Rotor Blades Made of Timken 17-22A(S) Steel. NACA RM E54F23a.

11. Moseson, Merland L., Krasner, Morton H., and Ziemer, Robert R.: Mechanical Design Analysis of Several Noncritical Air-Cooled Turbine Disks and a Corrugated-Insert Air-Cooled Turbine Rotor Blade. NACA RM E53E21, 1953.

12. Hubbartt, James E., Slone, Henry O., and Arne, Vernon L.: Method for Rapid Determination of Pressure Change for One-Dimensional Flow with Heat Transfer, Friction, Rotation, and Area Change. NACA TN 3150, 1954.

TABLE I. - SUMMARY OF RESULTS FOR SAMPLE CALCULATION

[Absolute minimum coolant flow, $w/(m+\tau)$, 0.0116.]

m	τ	Y	Minimum coolant flow, $\frac{w}{m+\tau}$
0.020	0.005	0.100	0.0190
	.010	.131	.0176
	.015	.143	.0169
0.035	0.005	0.093	0.0215
	.010	.103	.0204
	.015	.118	.0204
0.050	0.005	0.090	0.0258
	.010	.096	.0220
	.015	.100	.0207

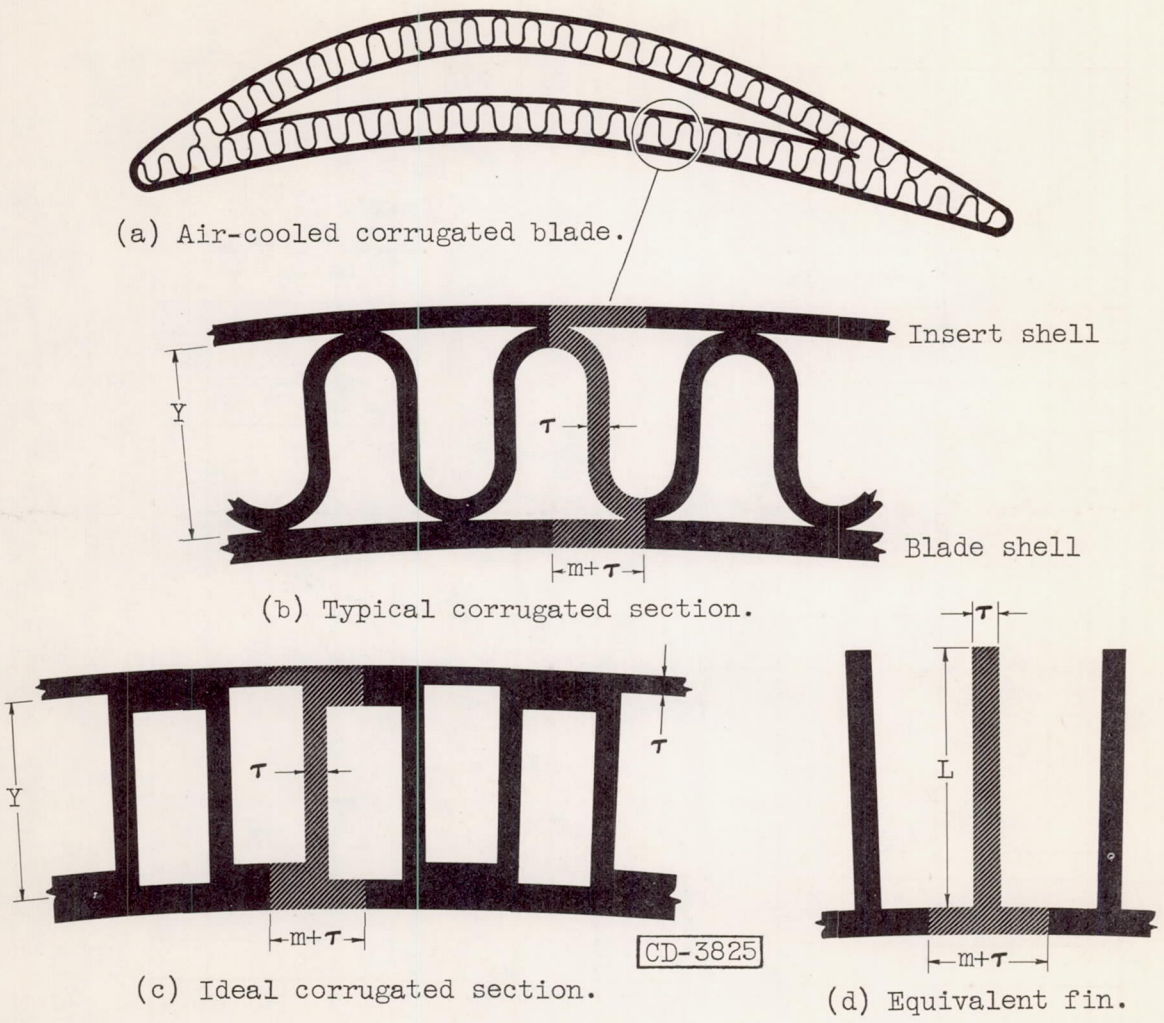

(a) Air-cooled corrugated blade.

(b) Typical corrugated section.

(c) Ideal corrugated section.

(d) Equivalent fin.

Figure 1. - Development of equivalent fin from typical corrugated section.

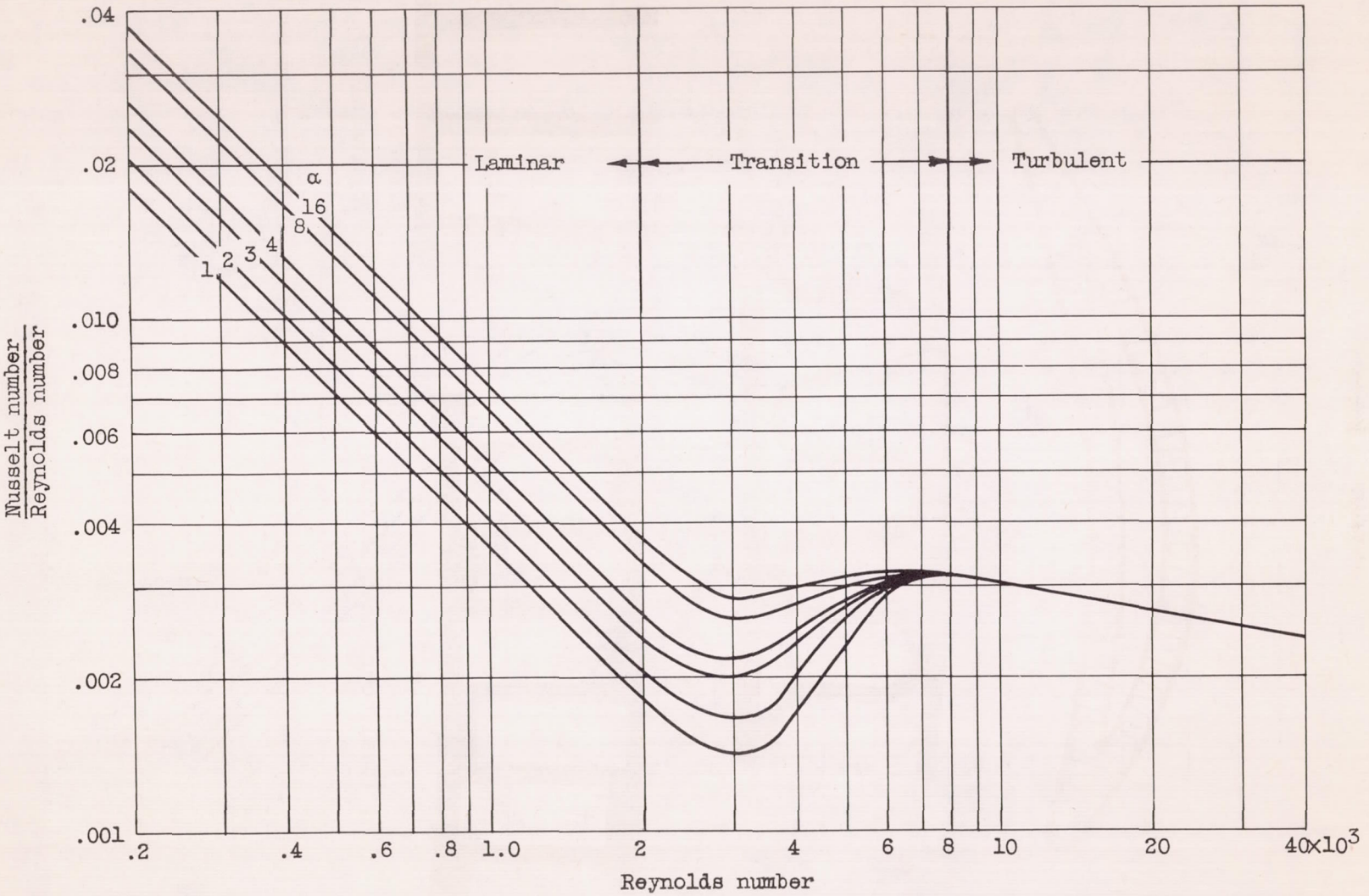

Figure 2. - Heat-transfer correlations.

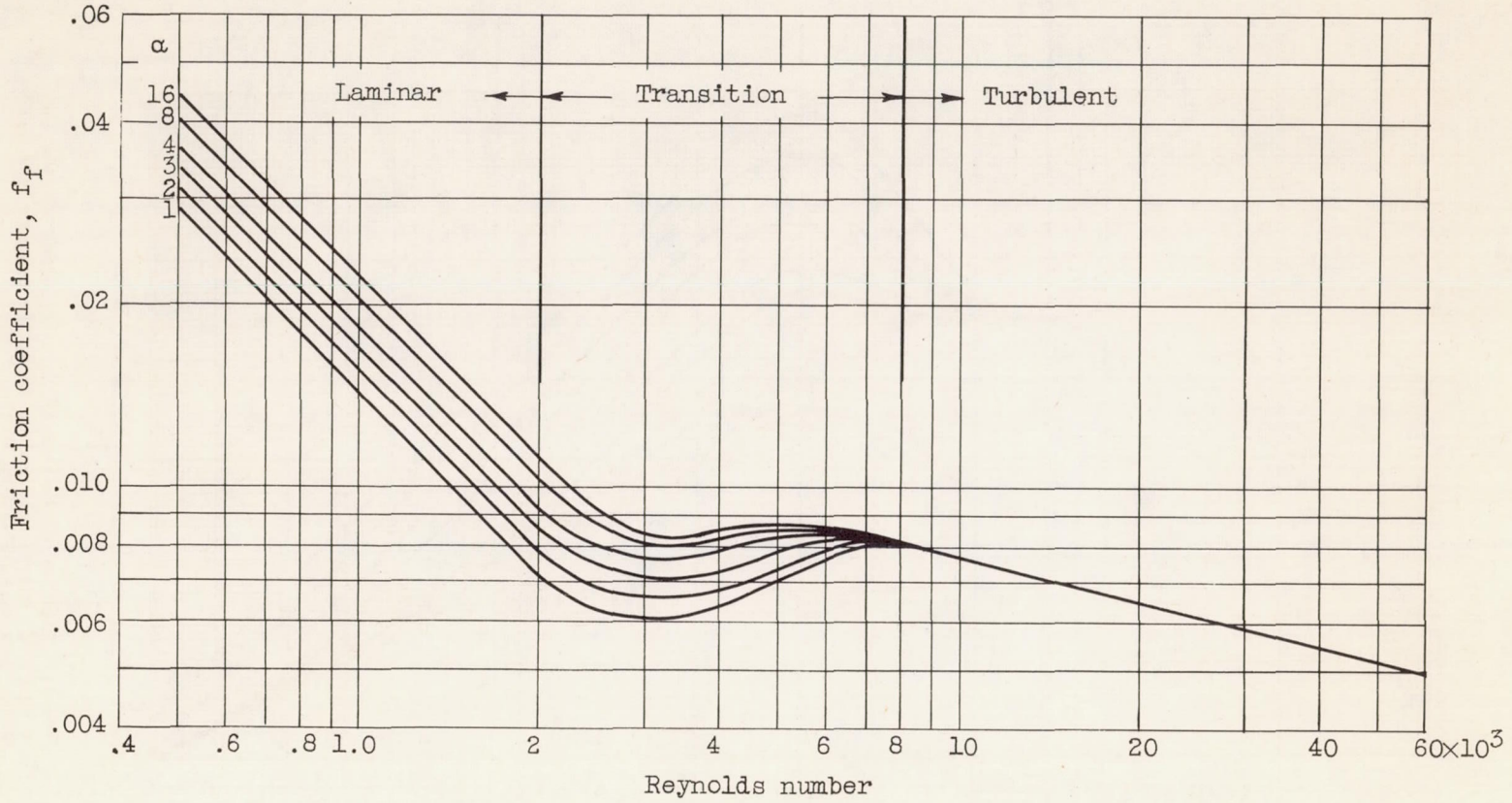

Figure 3. - Variation of friction coefficient with Reynolds number.

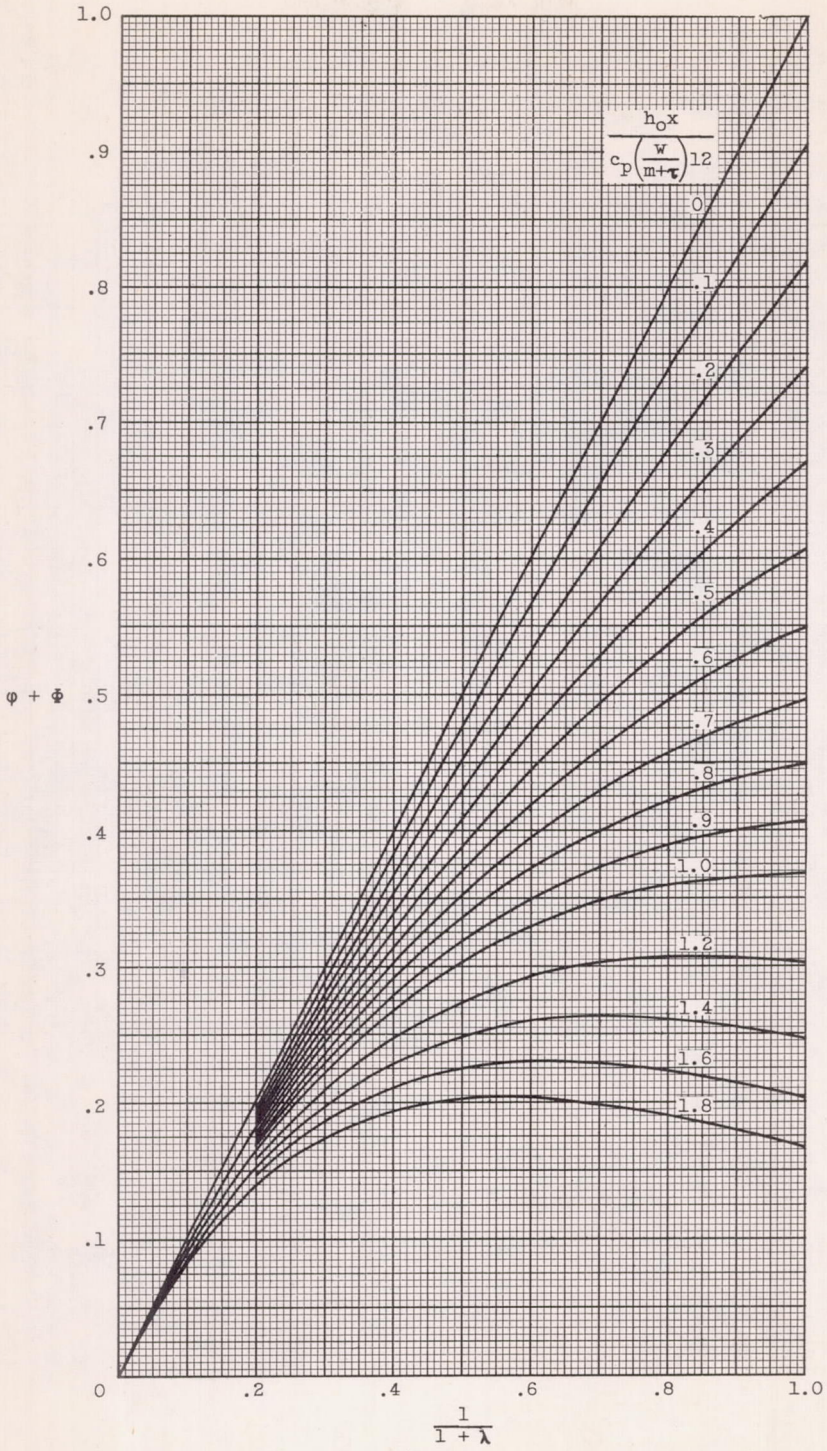

Figure 4. - Plot for evaluation of λ. (A larger working copy of this fig. may be obtained by using the request card bound in the back of this report.)

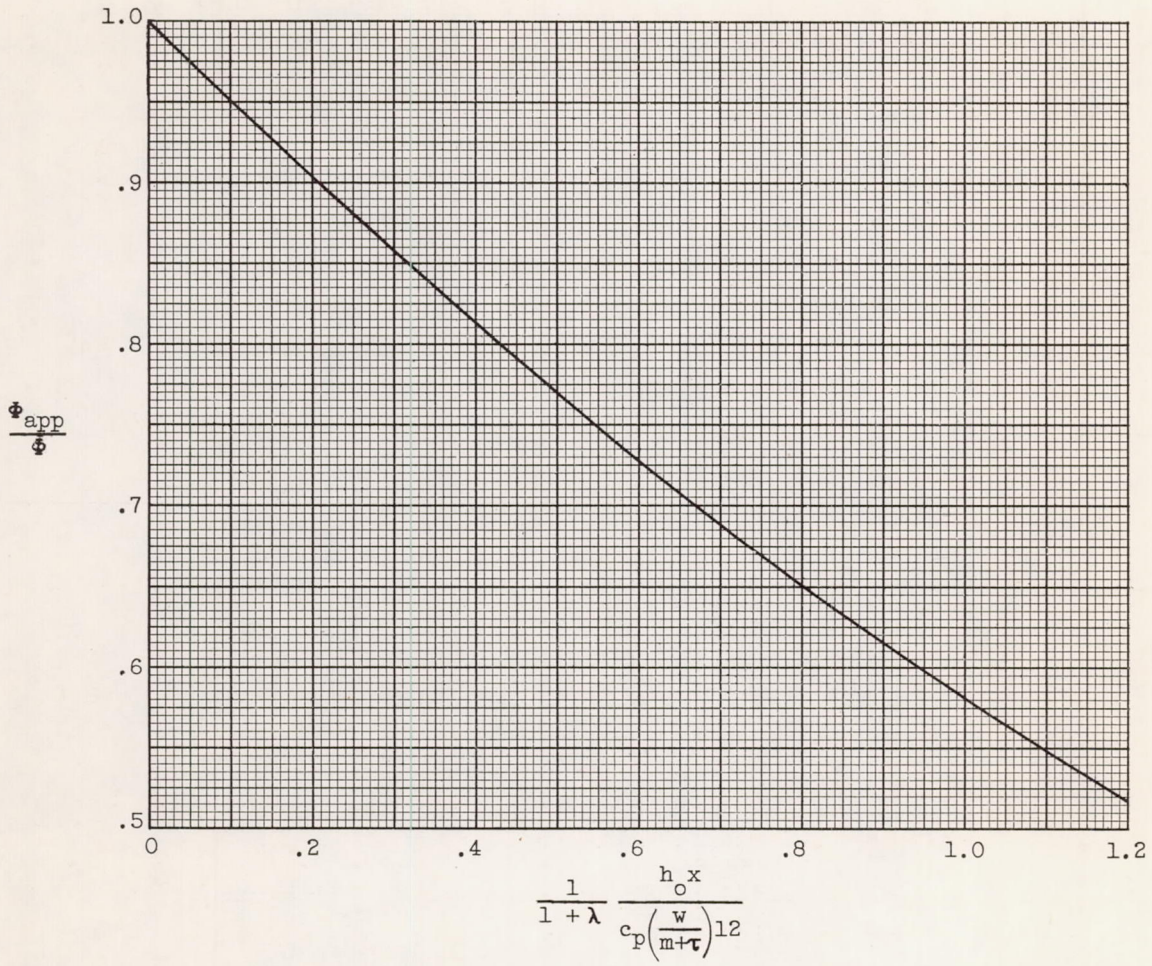

Figure 5. - Plot for evaluation of $\frac{\Phi_{app}}{\Phi}$.

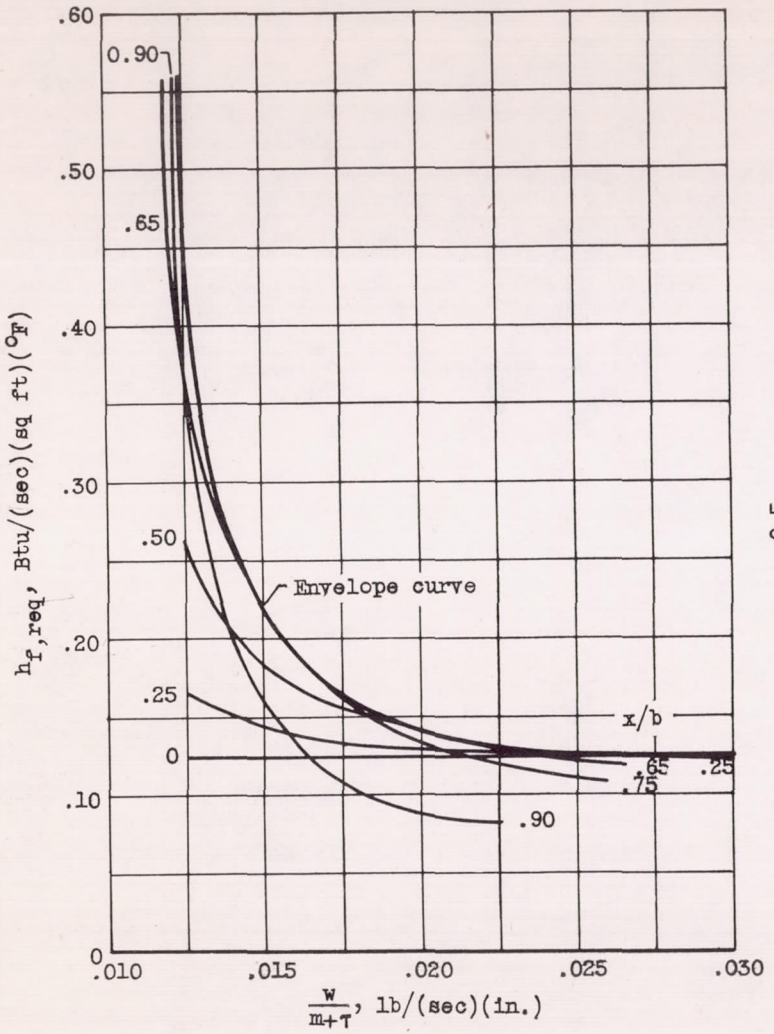

(a) Typical plot for development of envelope curve.

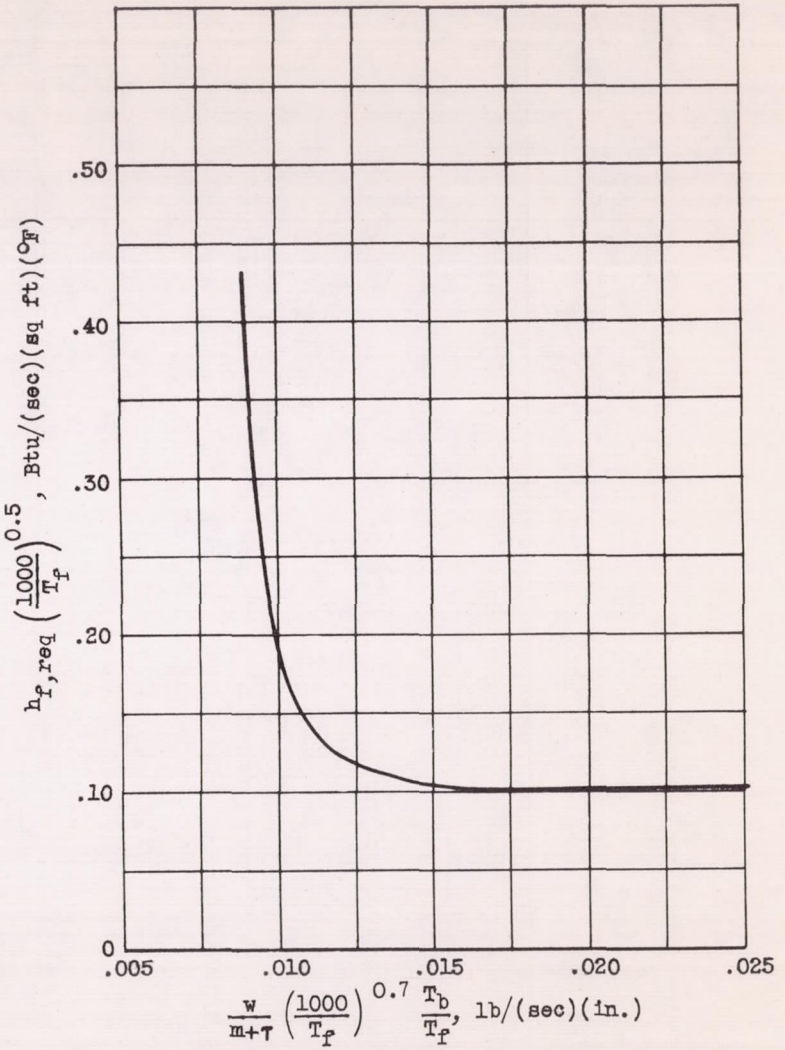

(b) Envelope curve plotted with coordinate system of charts.

Figure 6. - Development of $h_{f,req}$ curve for superimposition on charts.

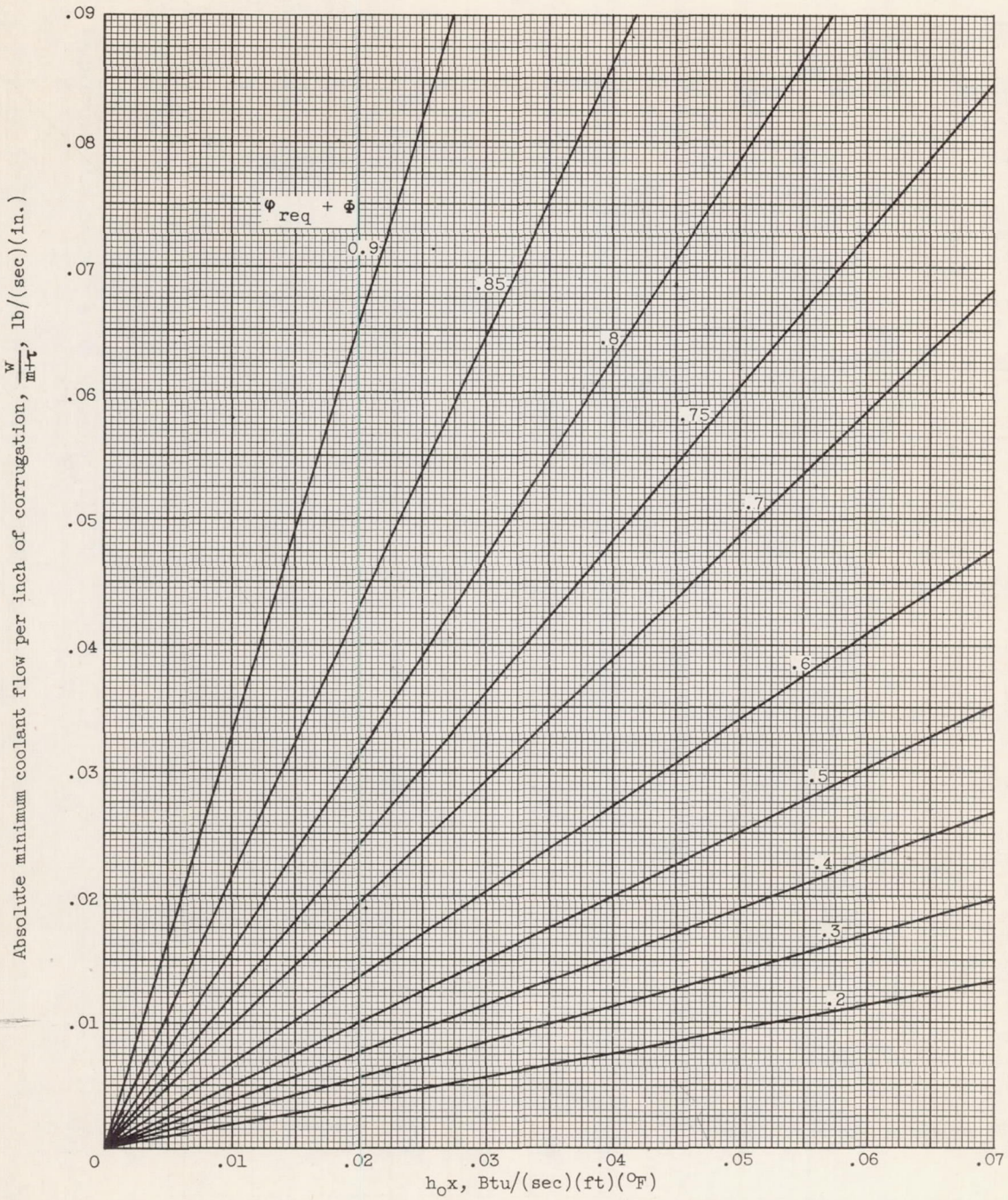

Figure 7. - Curves for evaluating absolute minimum required coolant flow per inch of corrugation.

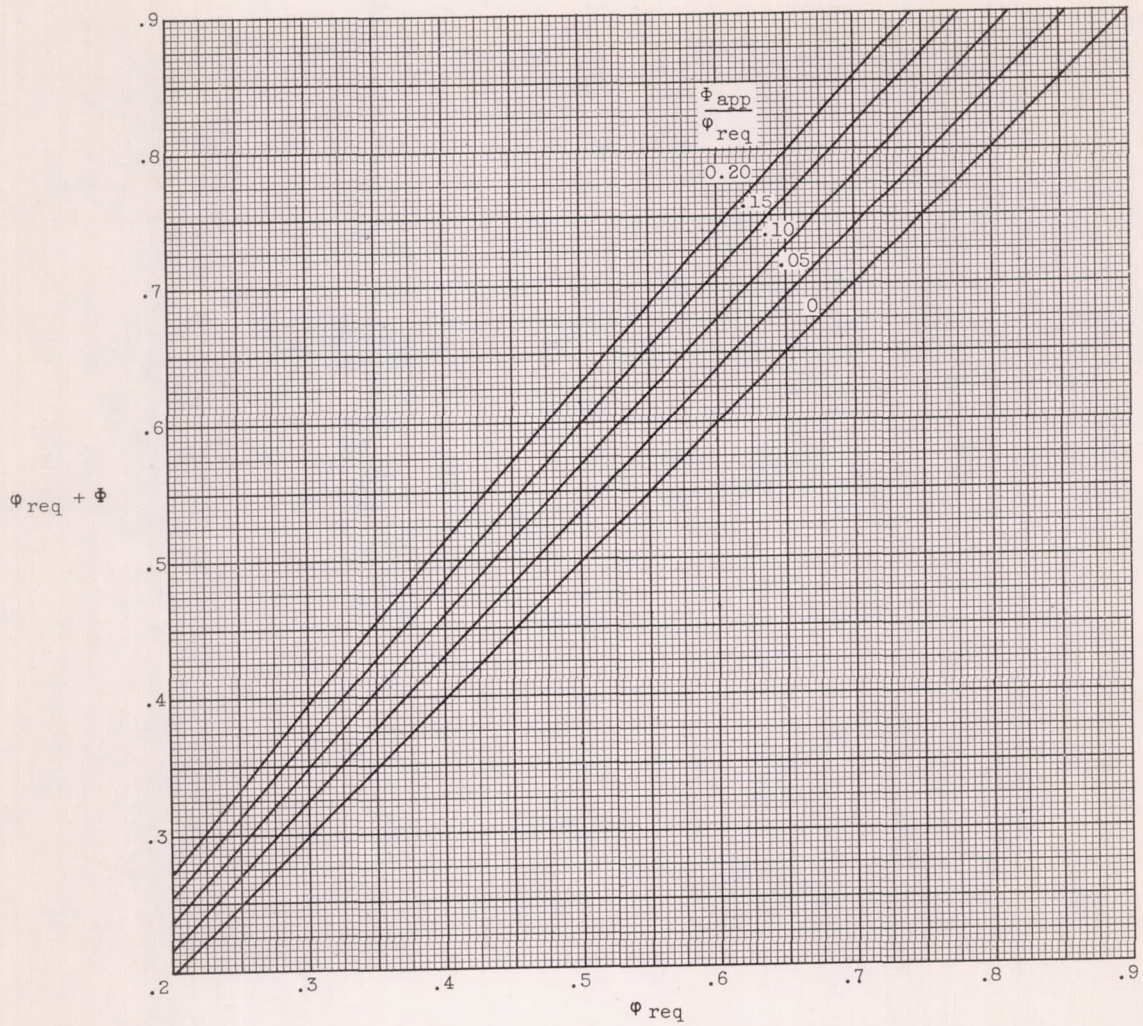

Figure 8. - Variation of $\varphi_{req} + \Phi$ with φ_{req} for absolute minimum required coolant flow per inch of corrugation.

Chart I

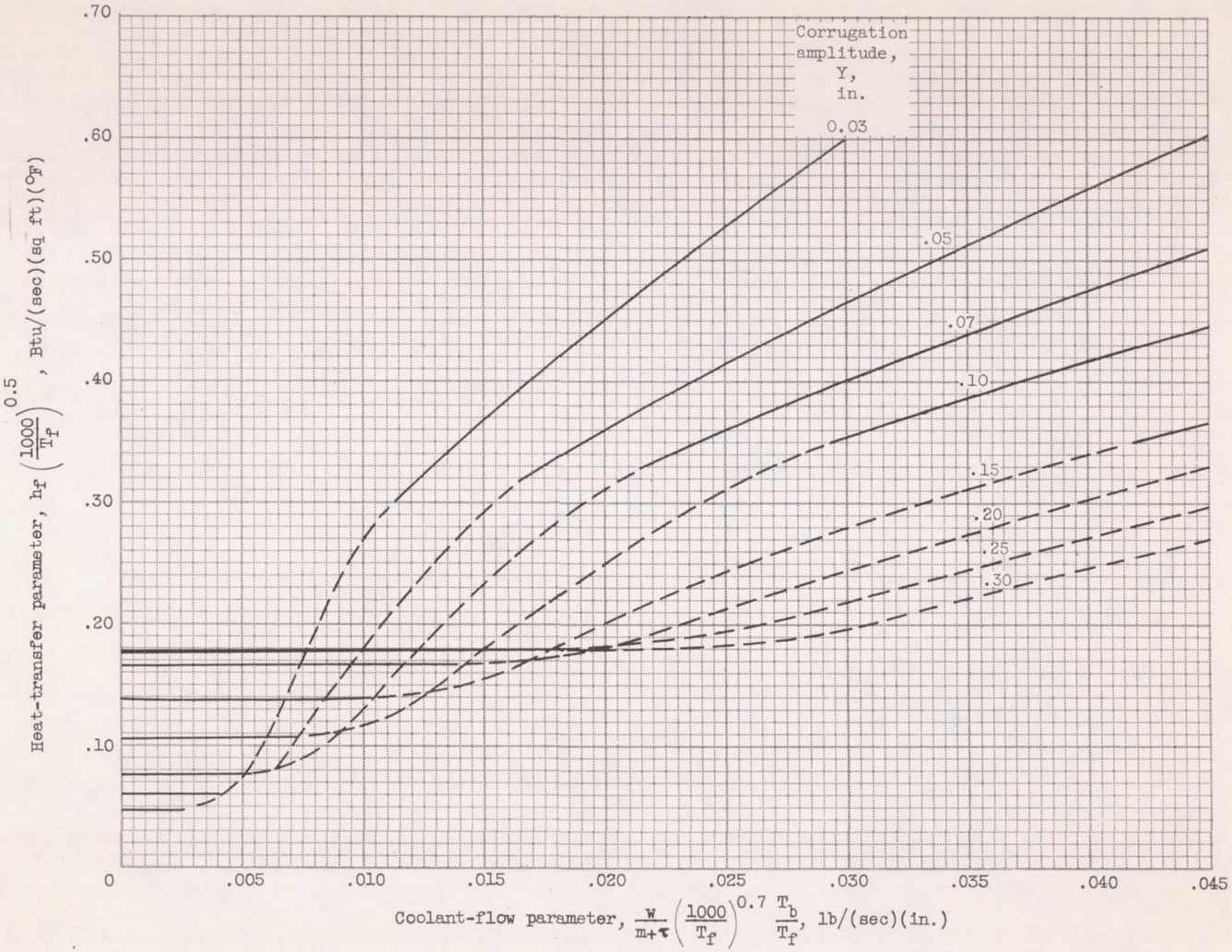

(a) Fin spacing, 0.020 inch; fin thickness, 0.005 inch.

Chart I. - Variation of heat-transfer parameter with coolant-flow parameter for $\left(\frac{16}{K}\right)\left(\frac{T_f}{1000}\right)^{0.5} = 0.5$.

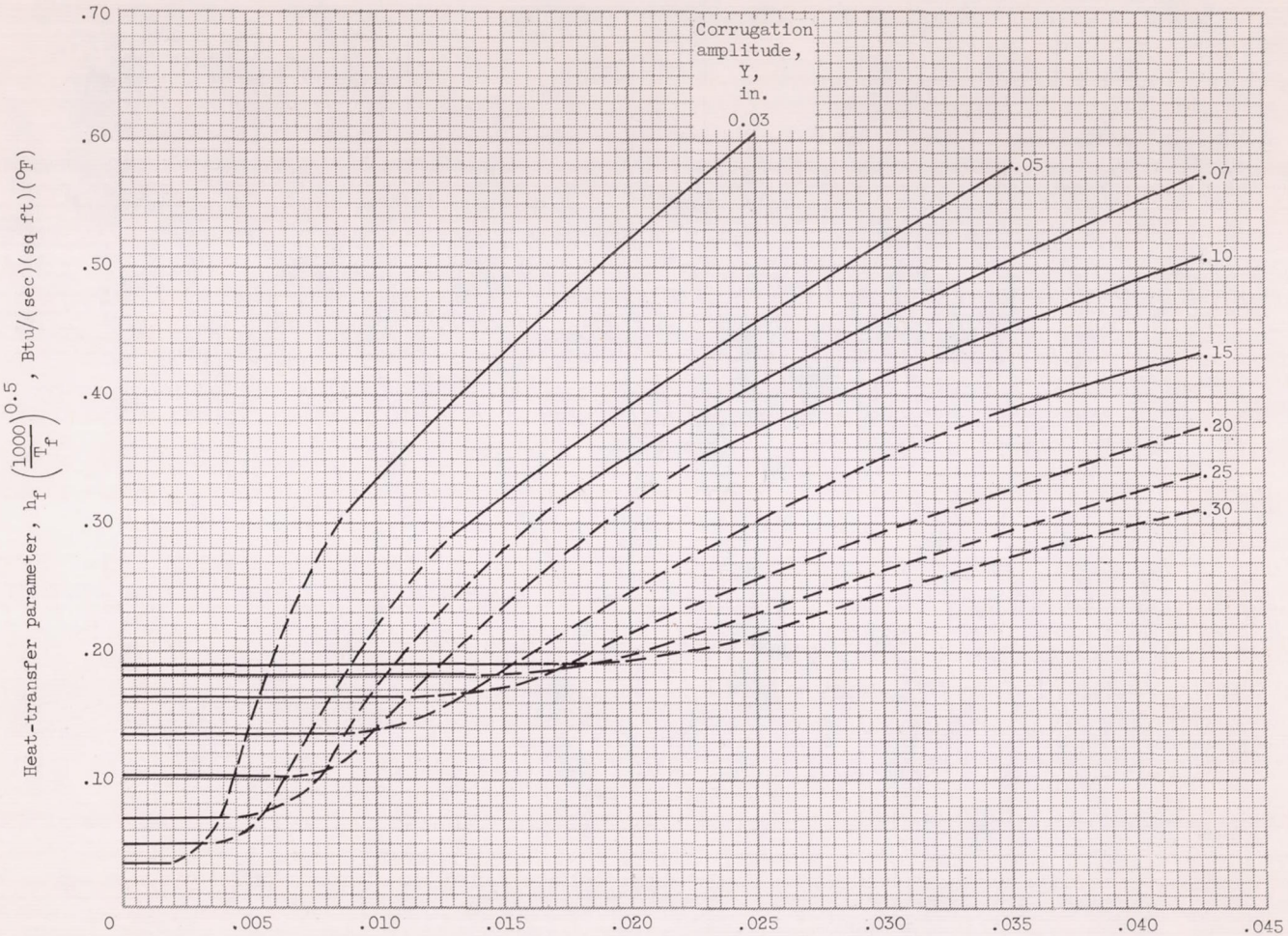

(b) Fin spacing, 0.020 inch; fin thickness, 0.010 inch.

Chart I. - Continued. Variation of heat-transfer parameter with coolant-flow parameter for $\left(\frac{16}{K}\right)\left(\frac{T_f}{1000}\right)^{0.5} = 0.5$.

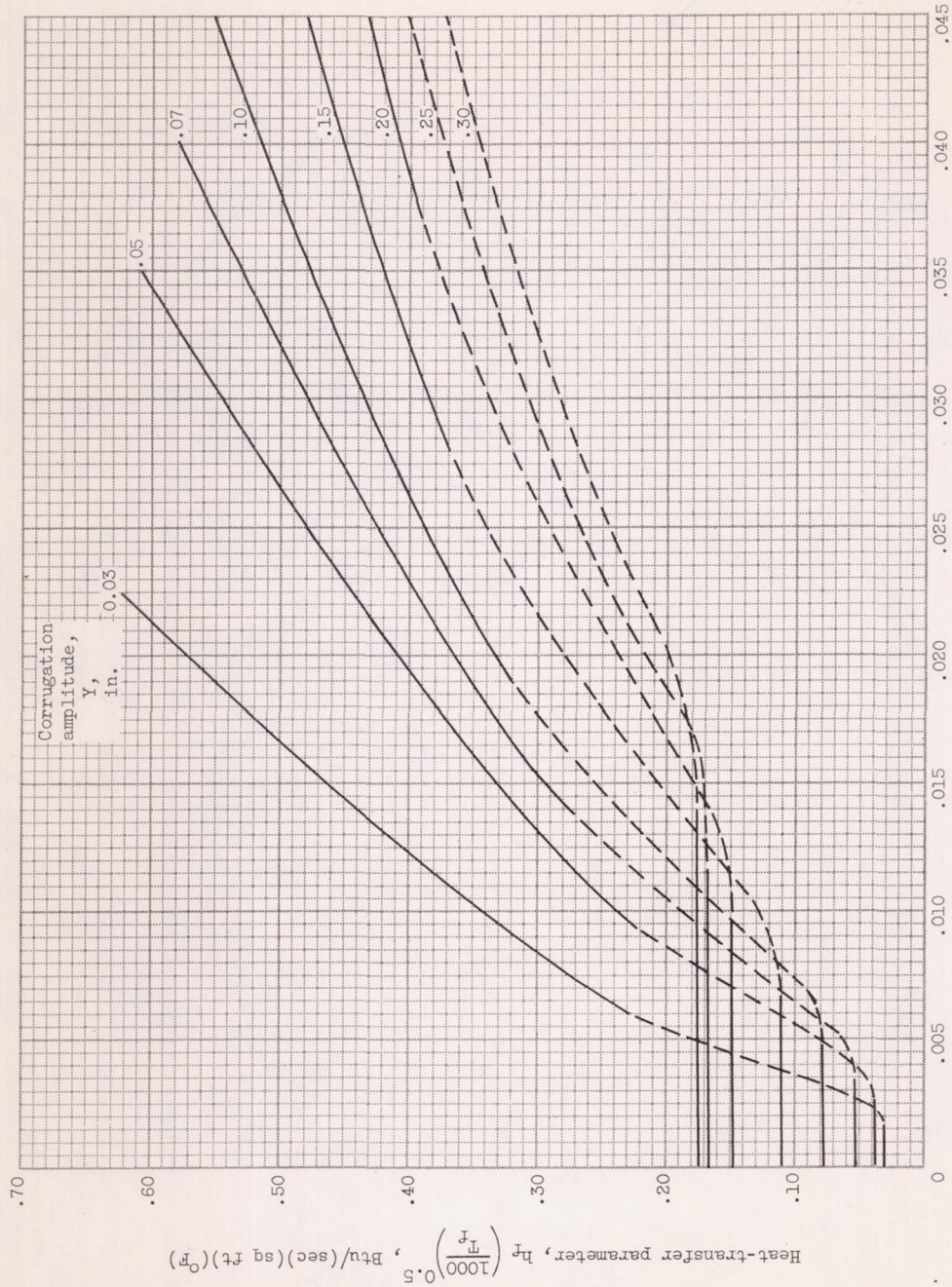

(c) Fin spacing, 0.020 inch; fin thickness, 0.015 inch.

Chart I. - Continued. Variation of heat-transfer parameter with coolant-flow parameter for $\left(\frac{16}{K}\right)\left(\frac{T_f}{1000}\right)^{0.5} = 0.5$.

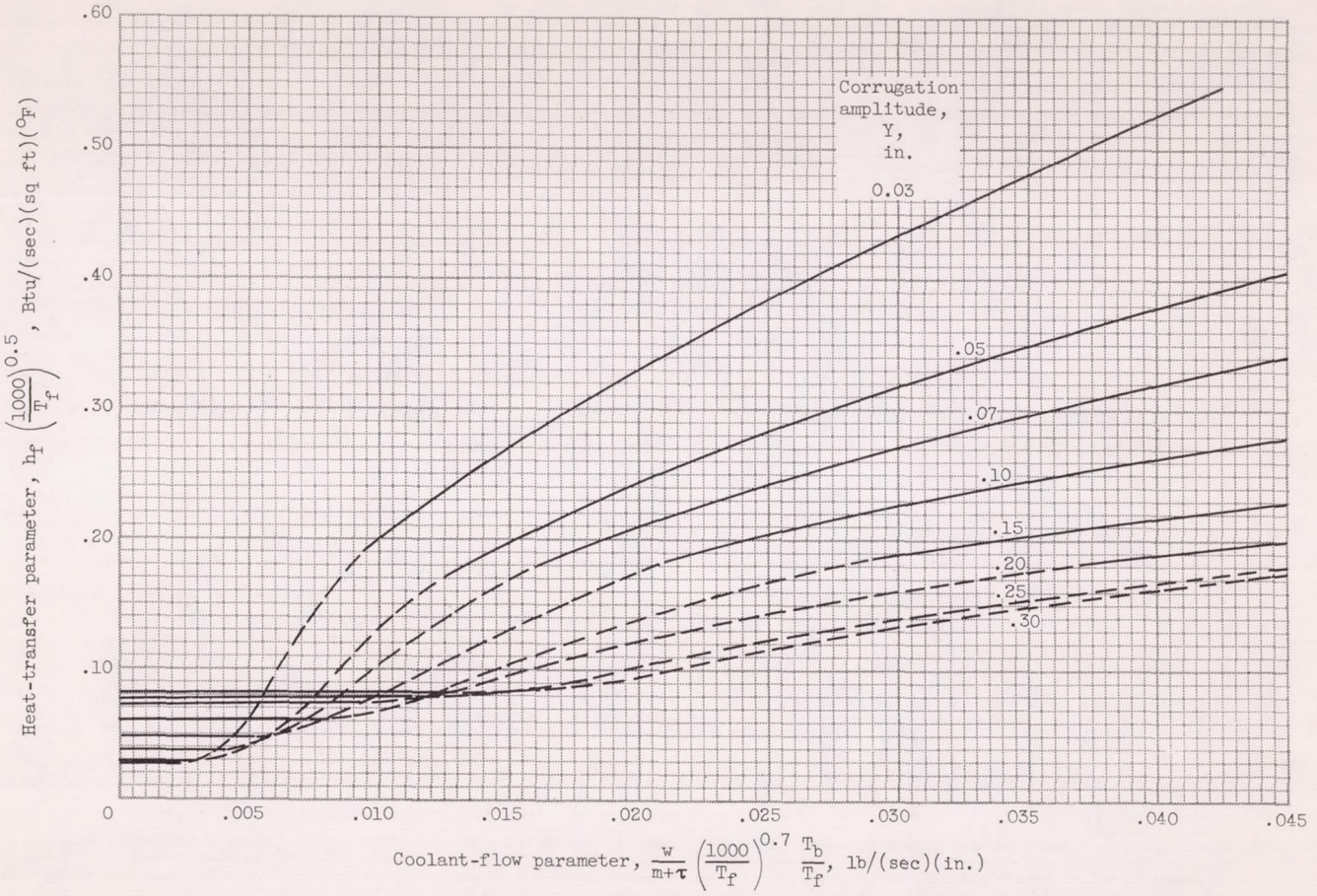

(d) Fin spacing, 0.035 inch; fin thickness, 0.005 inch.

Chart I. - Continued. Variation of heat-transfer parameter with coolant-flow parameter for $\left(\frac{16}{K}\right)\left(\frac{T_f}{1000}\right)^{0.5} = 0.5$.

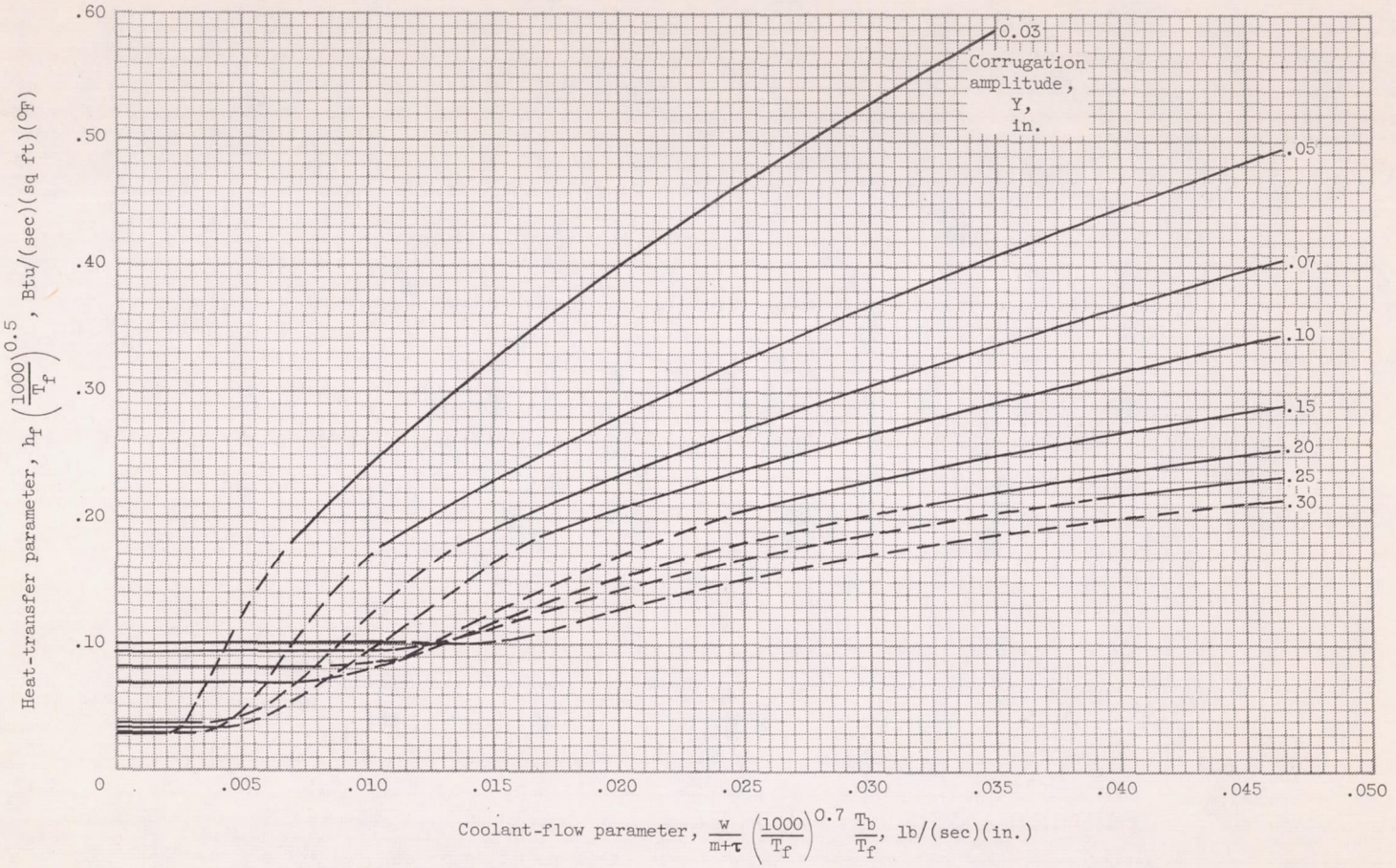

(e) Fin spacing, 0.035 inch; fin thickness, 0.010 inch.

Chart I. - Continued. Variation of heat-transfer parameter with coolant-flow parameter for $\left(\frac{16}{K}\right)\left(\frac{T_f}{1000}\right)^{0.5} = 0.5$.

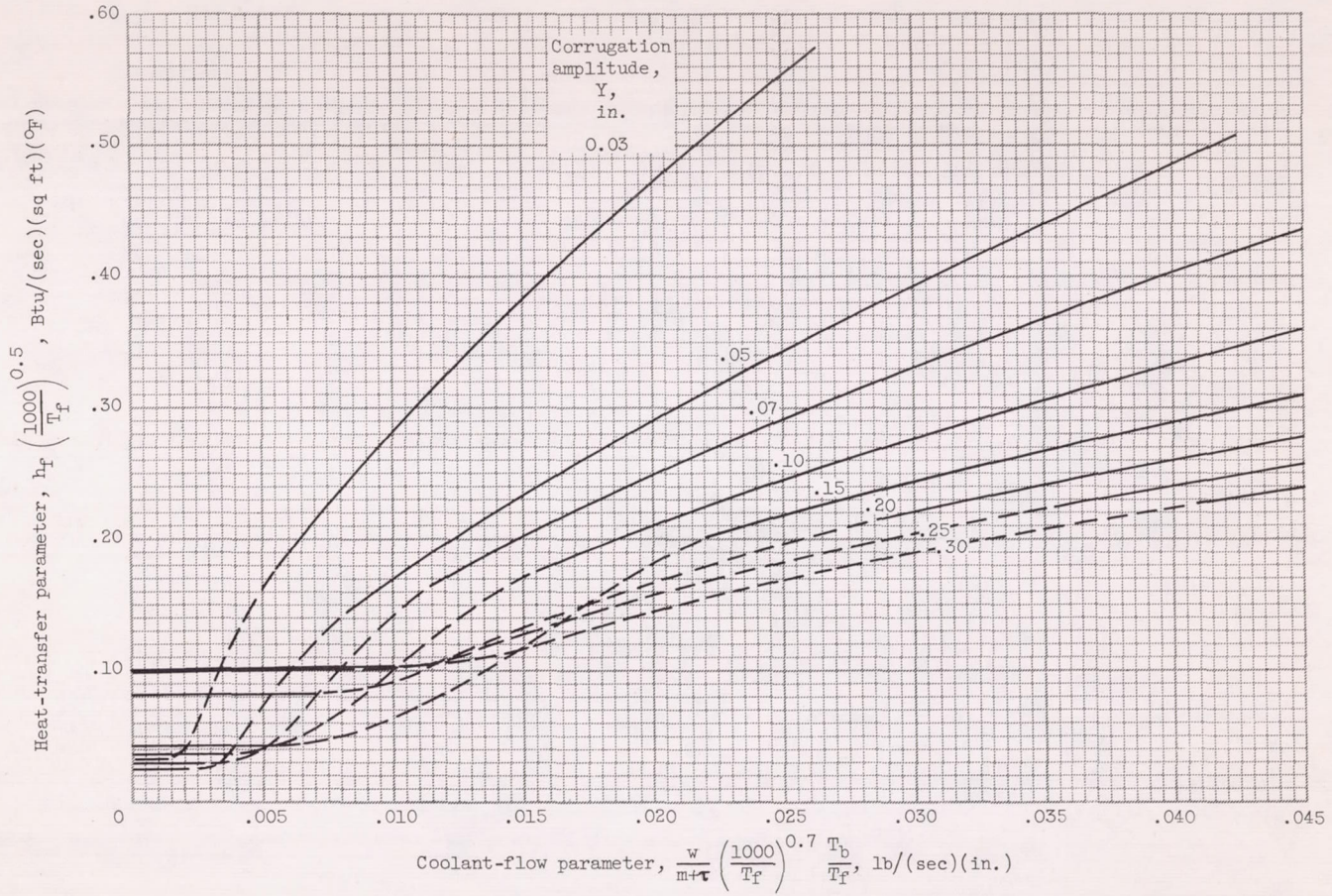

(f) Fin spacing, 0.035 inch; fin thickness, 0.015 inch.

Chart I. - Continued. Variation of heat-transfer parameter with coolant-flow parameter for $\left(\frac{16}{K}\right)\left(\frac{T_f}{1000}\right)^{0.5} = 0.5$.

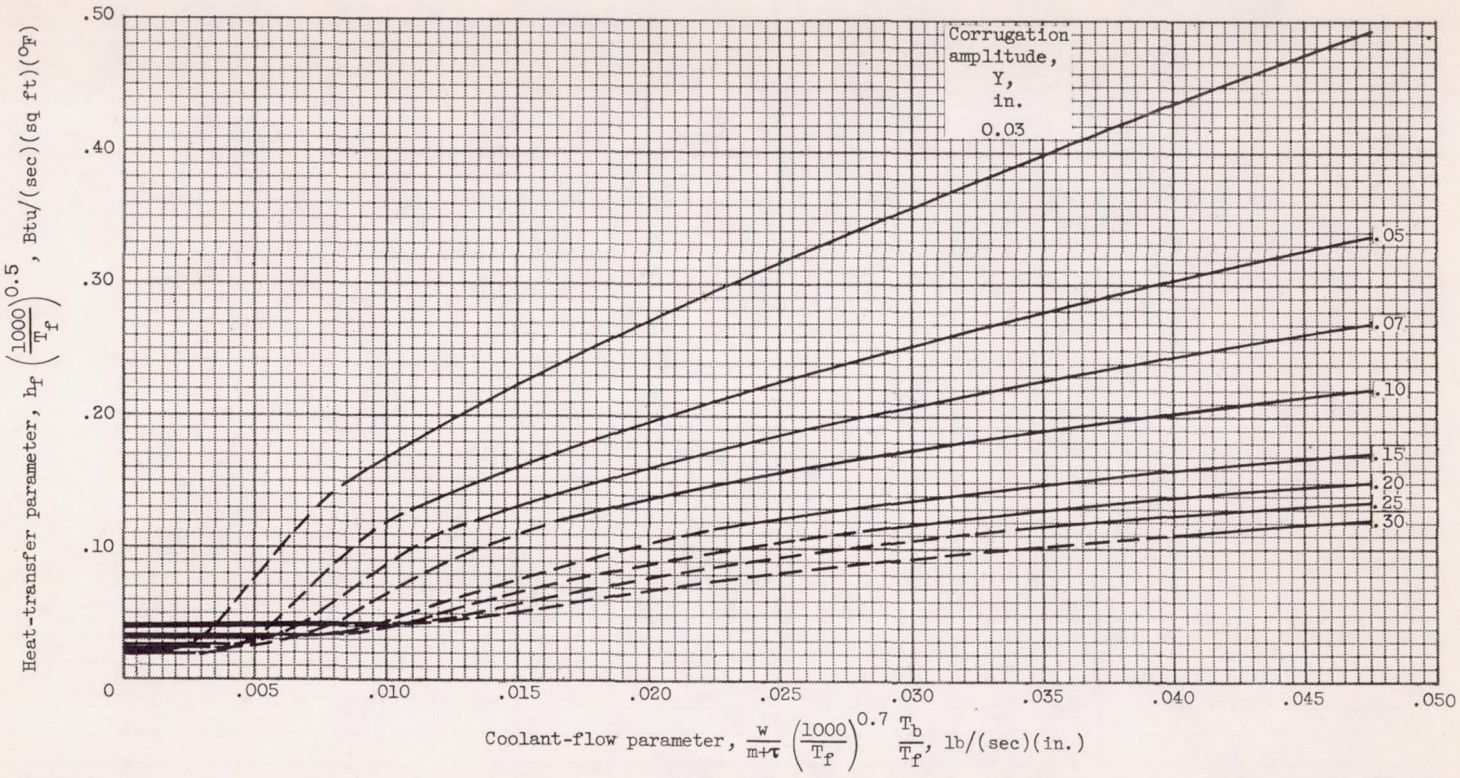

(g) Fin spacing, 0.050 inch; fin thickness, 0.005 inch.

Chart I. - Continued. Variation of heat-transfer parameter with coolant-flow parameter for $\left(\frac{16}{K}\right)\left(\frac{T_f}{1000}\right)^{0.5} = 0.5$.

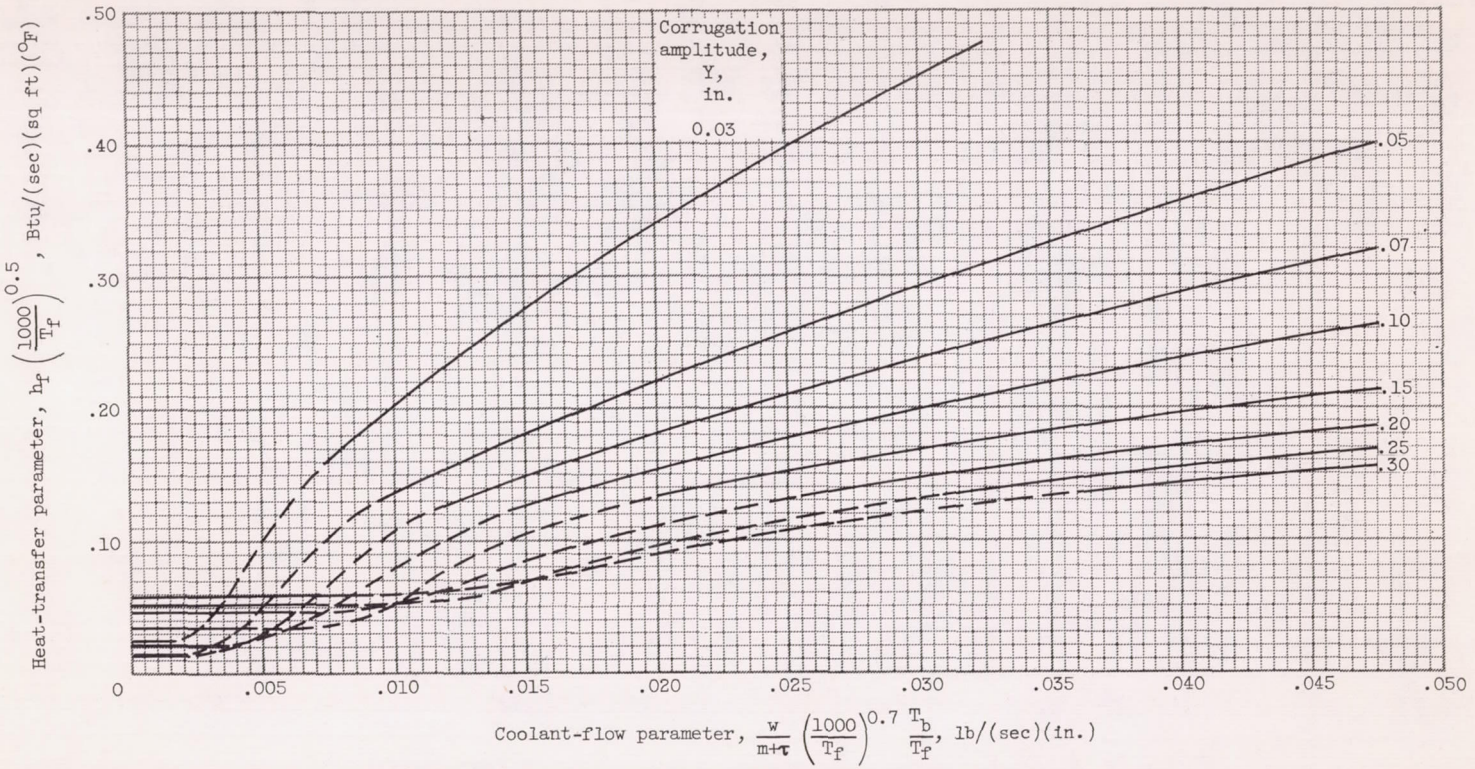

(h) Fin spacing, 0.050 inch; fin thickness, 0.010 inch.

Chart I. - Continued. Variation of heat-transfer parameter with coolant-flow parameter for $\left(\frac{16}{K}\right)\left(\frac{T_f}{1000}\right)^{0.5} = 0.5$.

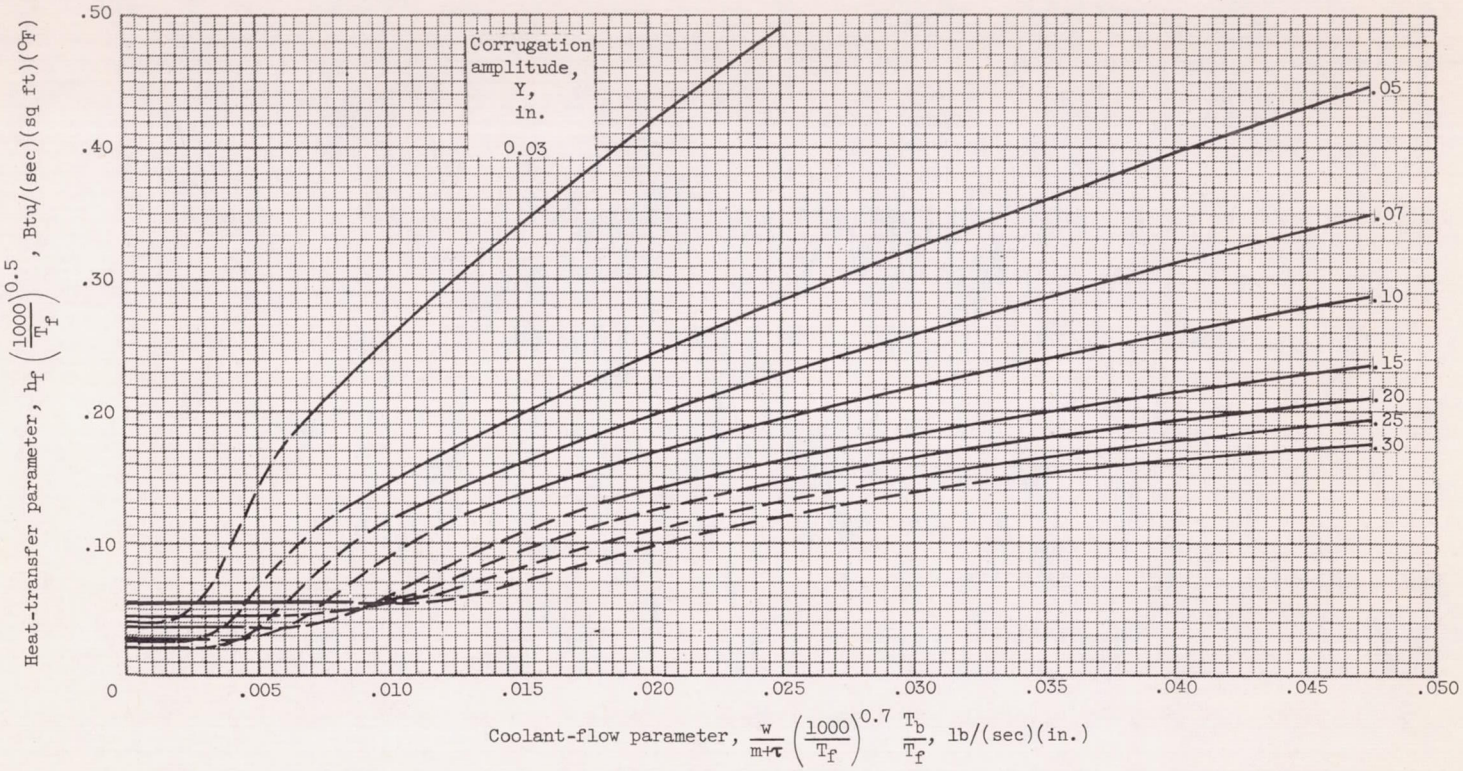

(i) Fin spacing, 0.050 inch; fin thickness, 0.015 inch.

Chart I. - Concluded. Variation of heat-transfer parameter with coolant-flow parameter for $\left(\frac{16}{K}\right)\left(\frac{T_f}{1000}\right)^{0.5} = 0.5$.

Chart II

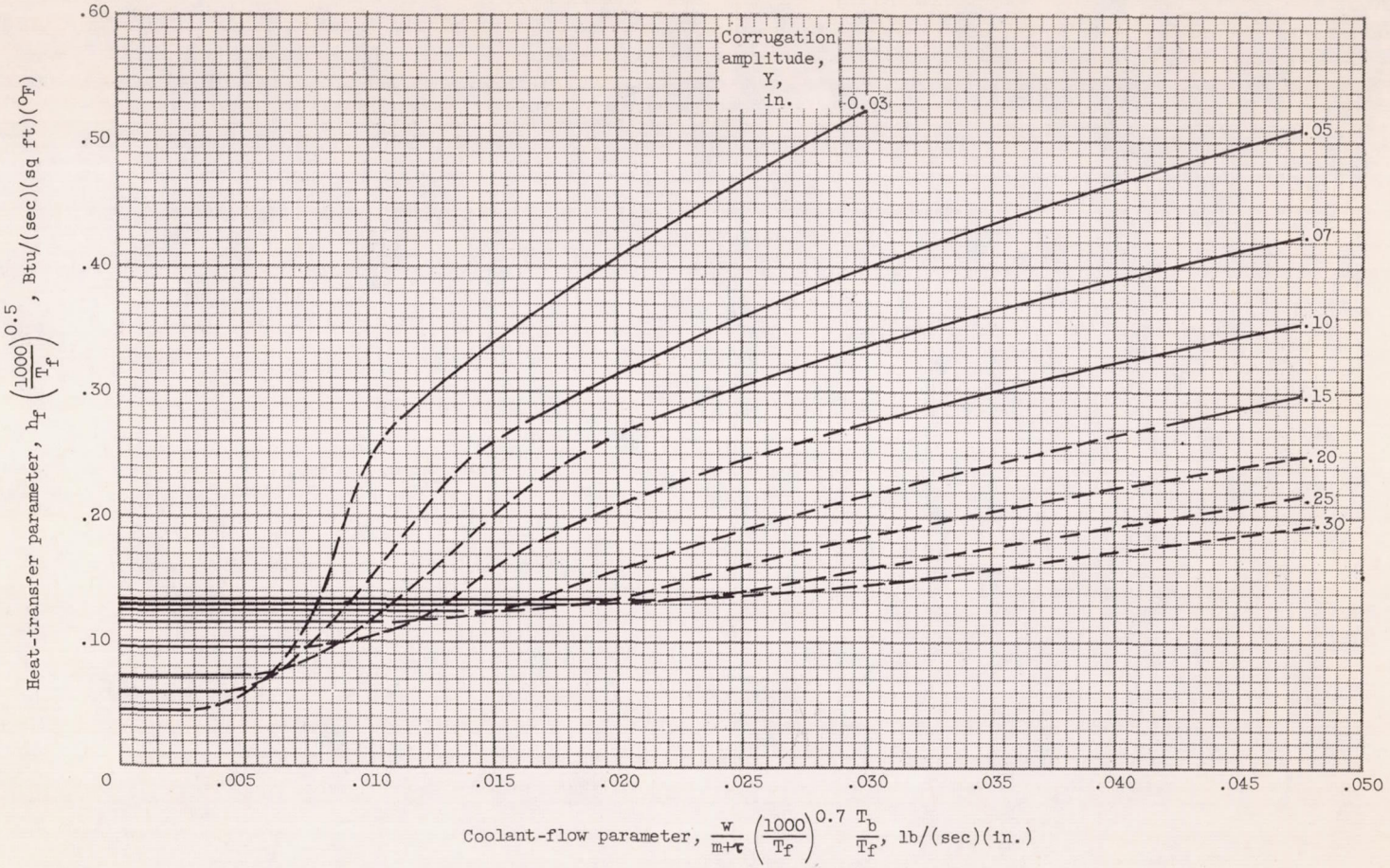

(a) Fin spacing, 0.020 inch; fin thickness, 0.005 inch.

Chart II. - Variation of heat-transfer parameter with coolant-flow parameter for $\left(\frac{16}{K}\right)\left(\frac{T_f}{1000}\right)^{0.5} = 1.0$.

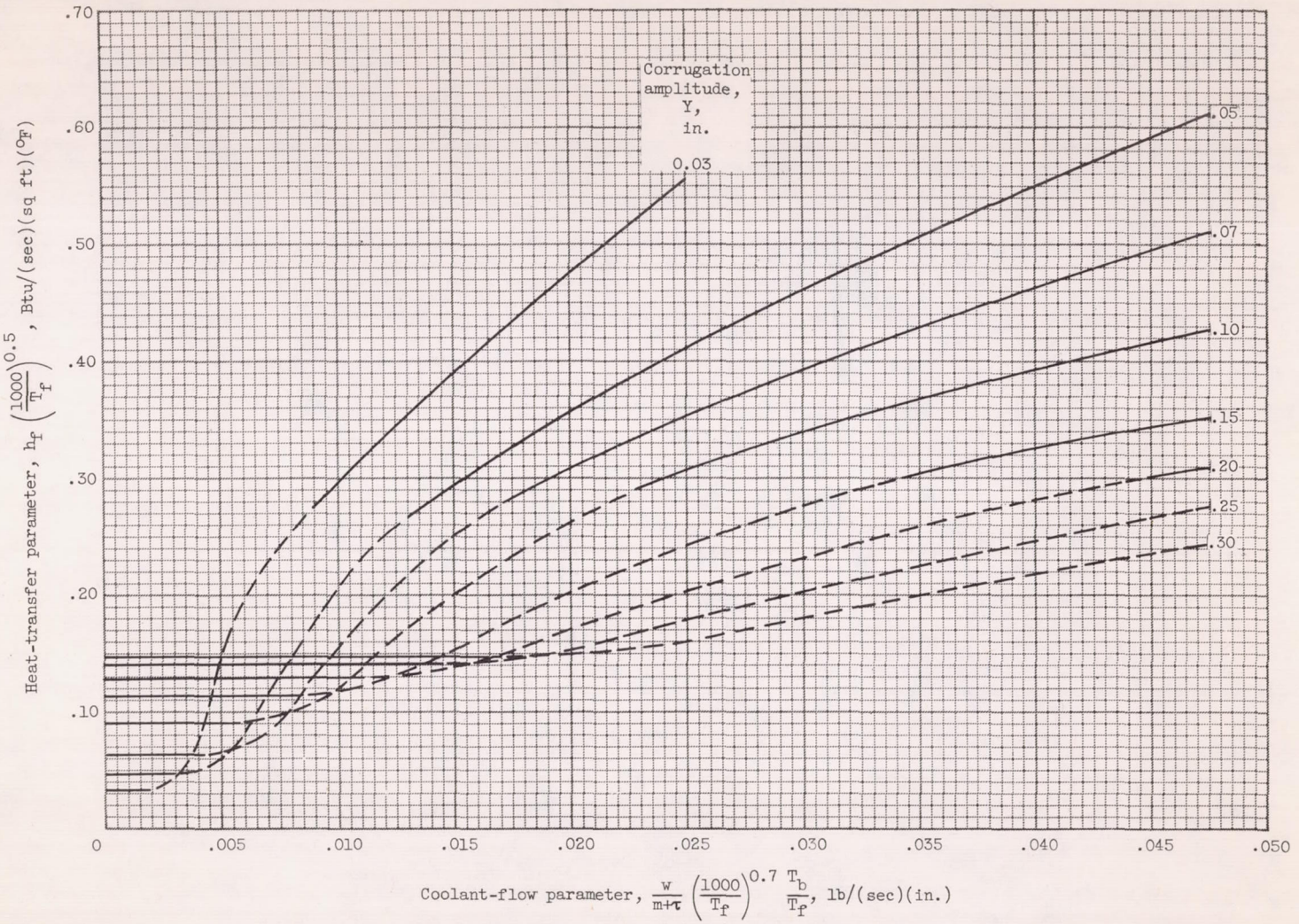

(b) Fin spacing, 0.020 inch; fin thickness, 0.010 inch.

Chart II. - Continued. Variation of heat-transfer parameter with coolant-flow parameter for $\left(\frac{16}{K}\right)\left(\frac{T_f}{1000}\right)^{0.5} = 1.0$.

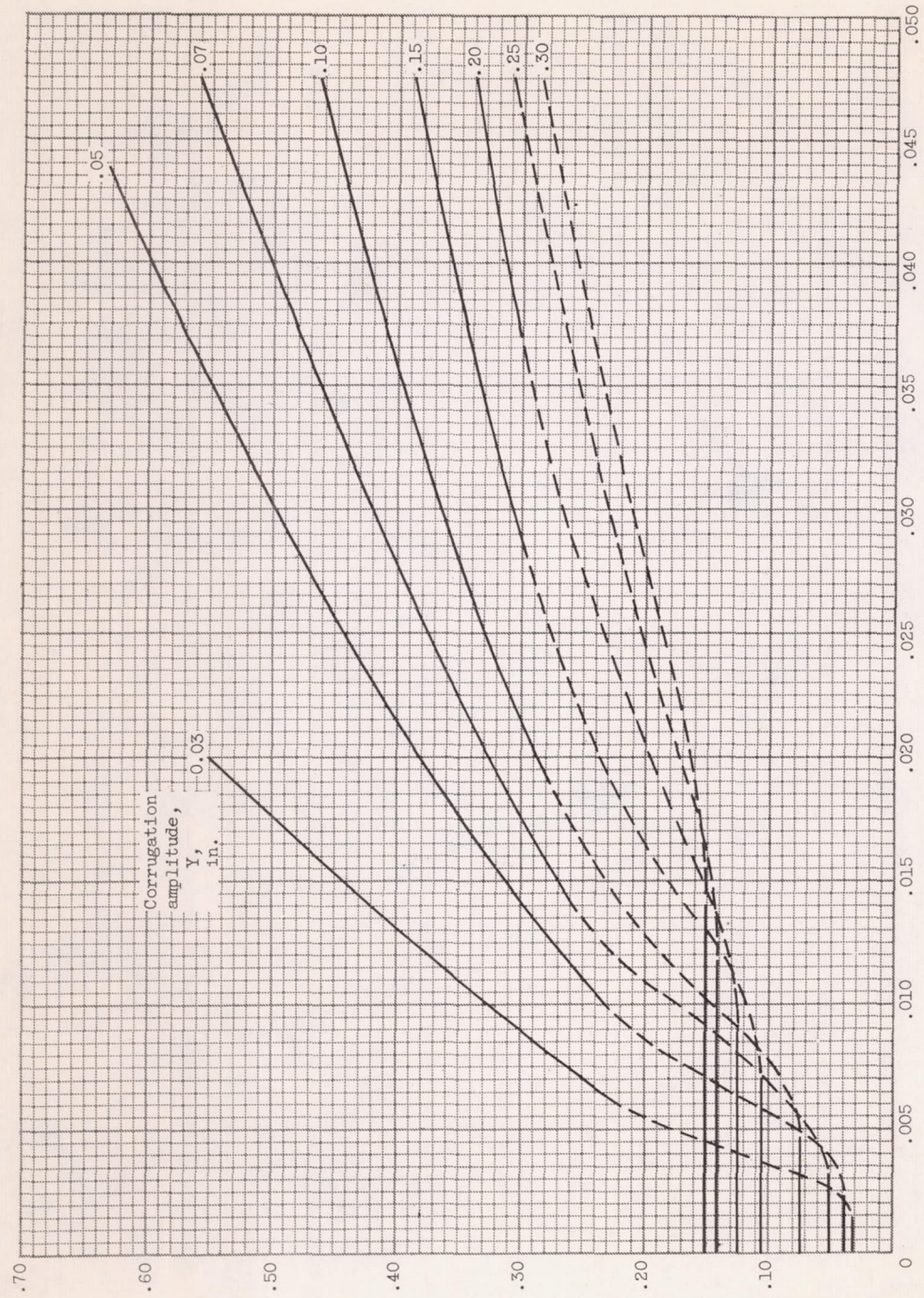

(c) Fin spacing, 0.020 inch; fin thickness, 0.015 inch.

Chart II. - Continued. Variation of heat-transfer parameter with coolant-flow parameter for $\left(\frac{1\hat{6}}{K}\right)\left(\frac{T_f}{1000}\right)^{0.5} = 1.0$

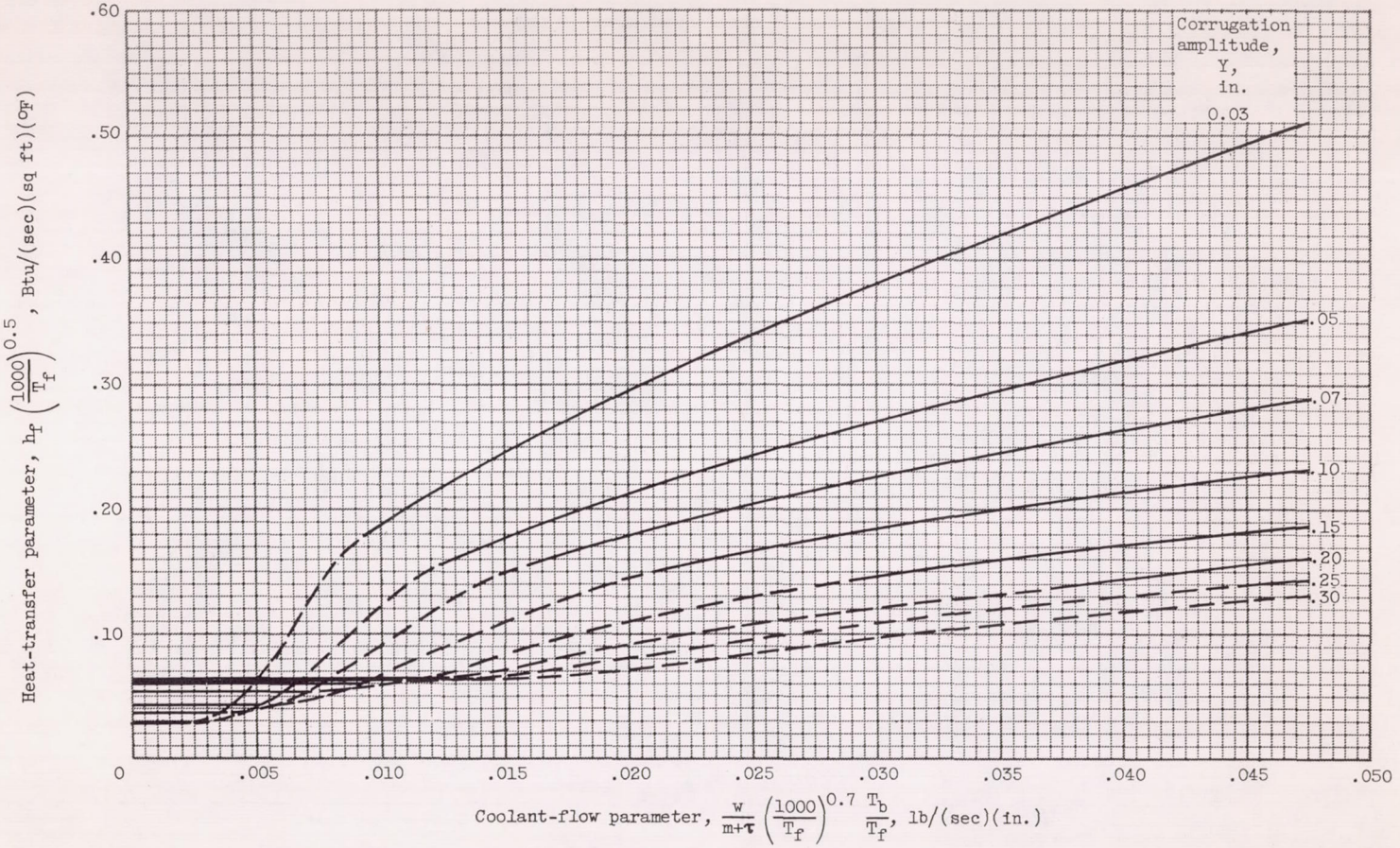

(d) Fin spacing, 0.035 inch; fin thickness, 0.005 inch.

Chart II. - Continued. Variation of heat-transfer parameter with coolant-flow parameter for $\left(\frac{16}{K}\right)\left(\frac{T_f}{1000}\right)^{0.5} = 1.0$.

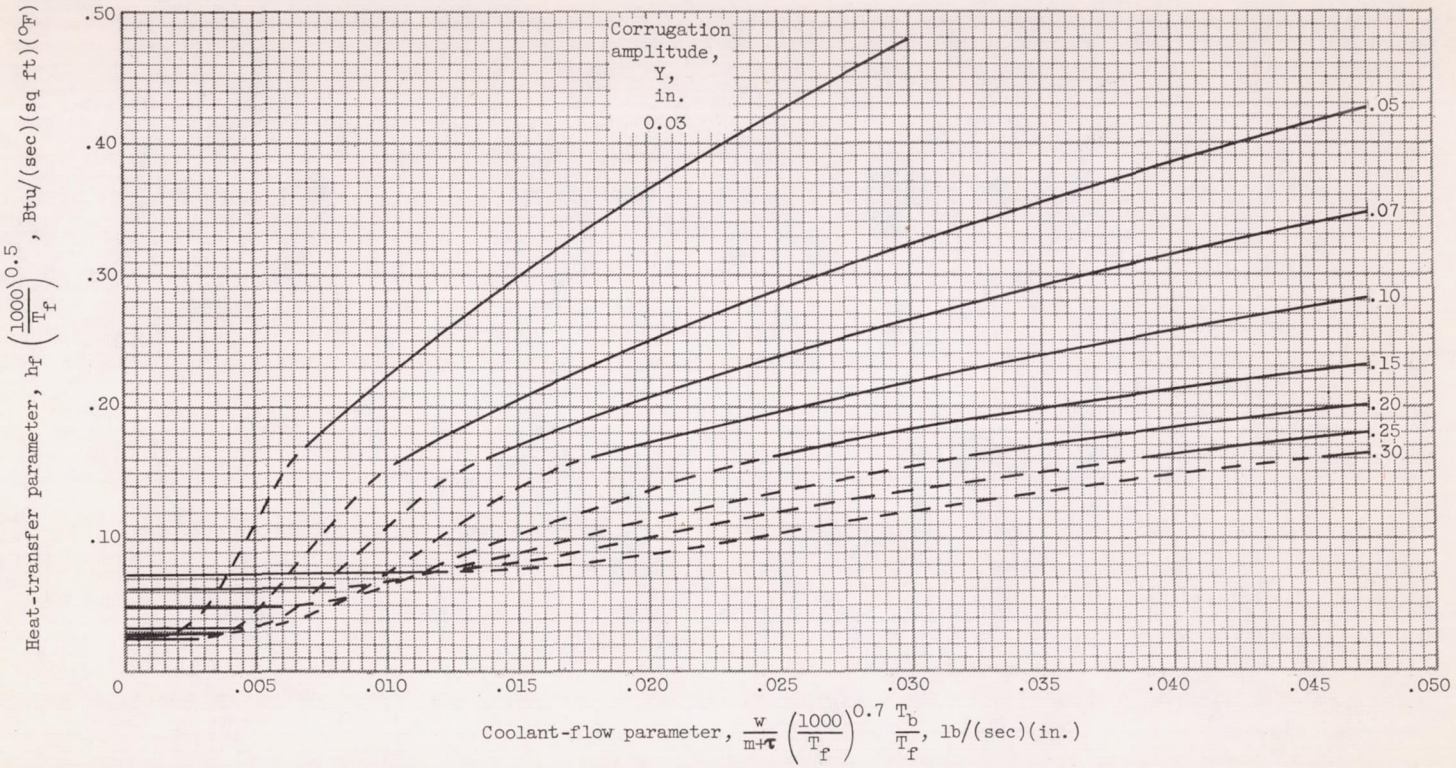

(e) Fin spacing, 0.035 inch; fin thickness, 0.010 inch.

Chart II. - Continued. Variation of heat-transfer parameter with coolant-flow parameter for $\left(\frac{16}{K}\right)\left(\frac{T_f}{1000}\right)^{0.5} = 1.0$.

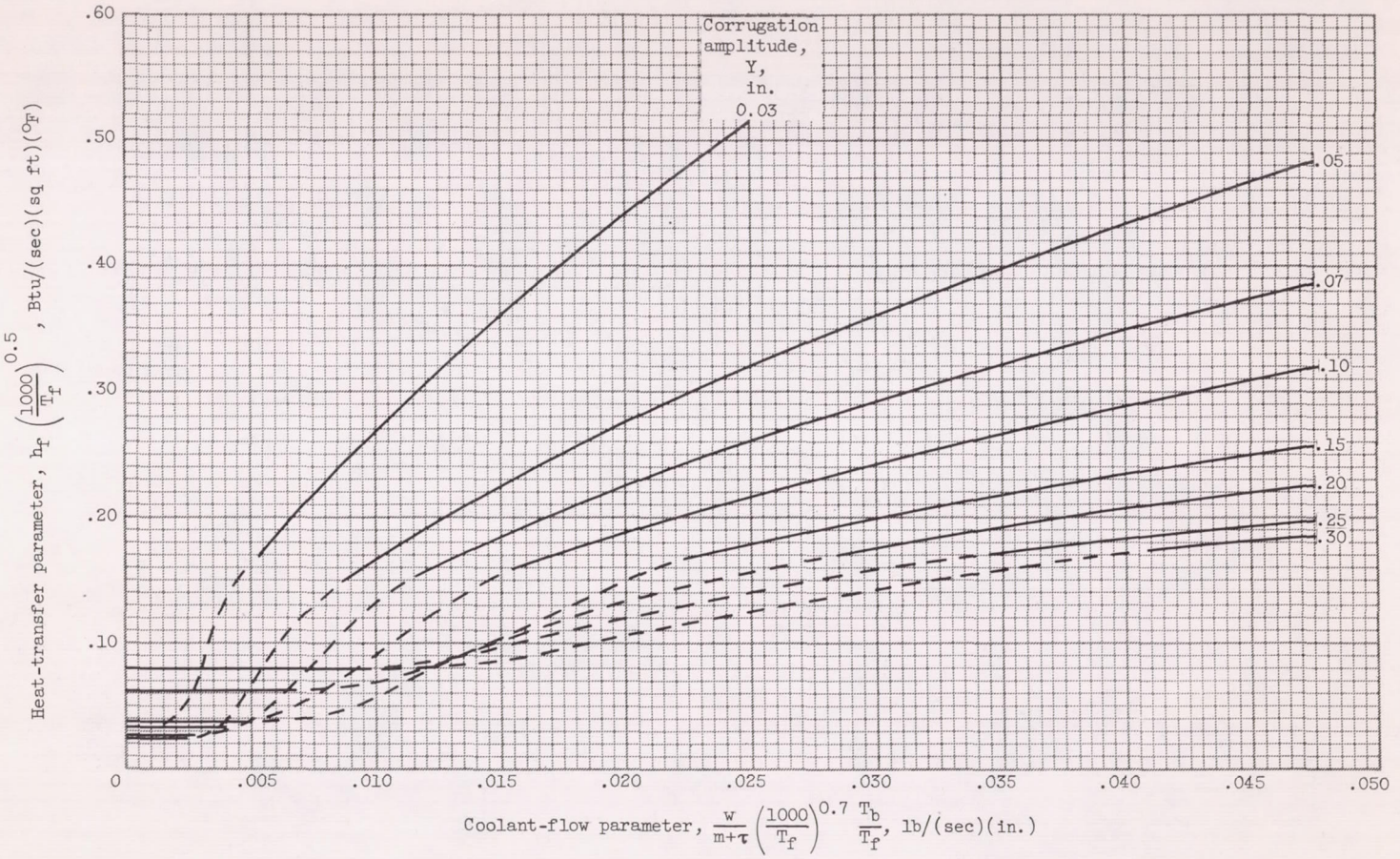

(f) Fin spacing, 0.035 inch; fin thickness, 0.015 inch.

Chart II. - Continued. Variation of heat-transfer parameter with coolant-flow parameter for $\left(\frac{16}{K}\right)\left(\frac{T_f}{1000}\right)^{0.5} = 1.0$.

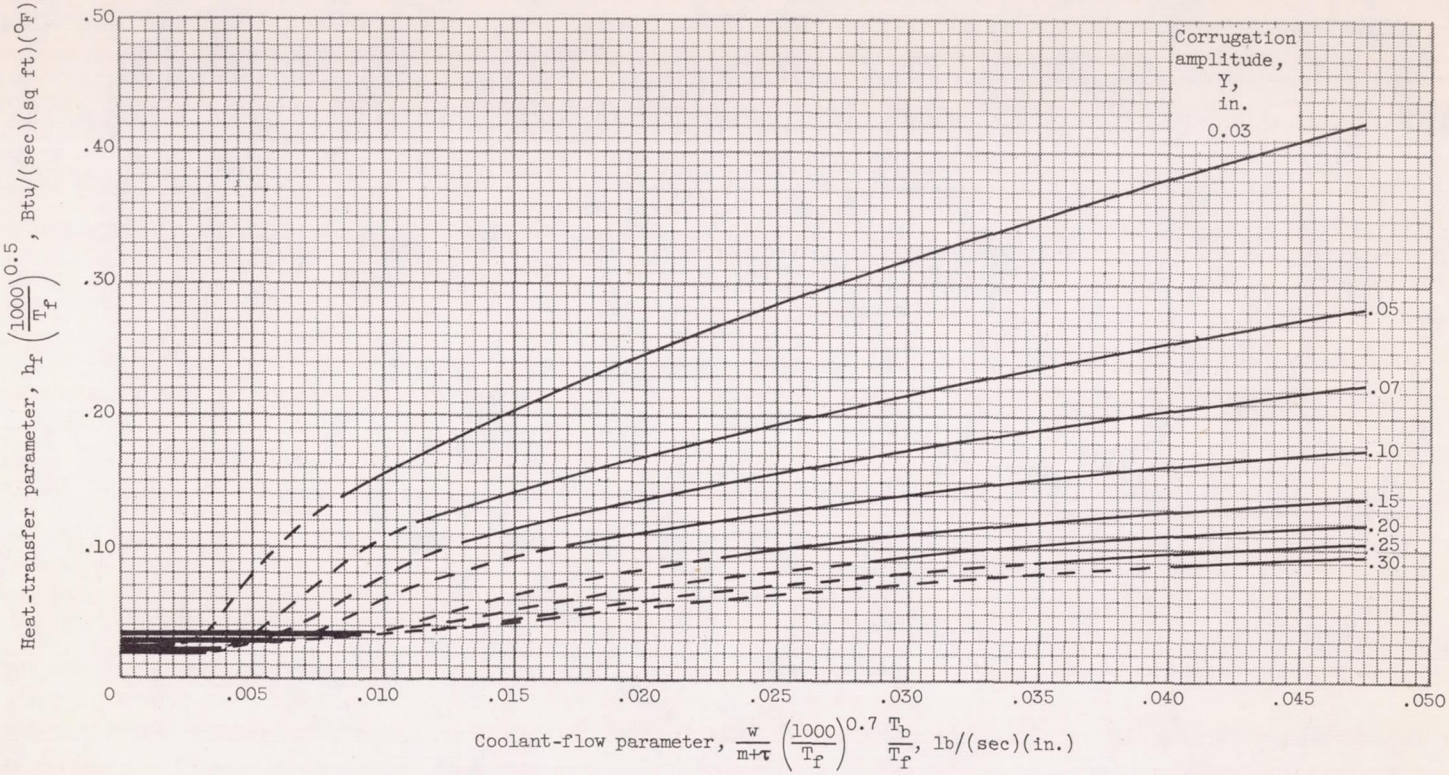

(g) Fin spacing, 0.050 inch; fin thickness, 0.005 inch.

Chart II. - Continued. Variation of heat-transfer parameter with coolant-flow parameter for $\left(\frac{16}{K}\right)\left(\frac{T_f}{1000}\right)^{0.5} = 1.0$.

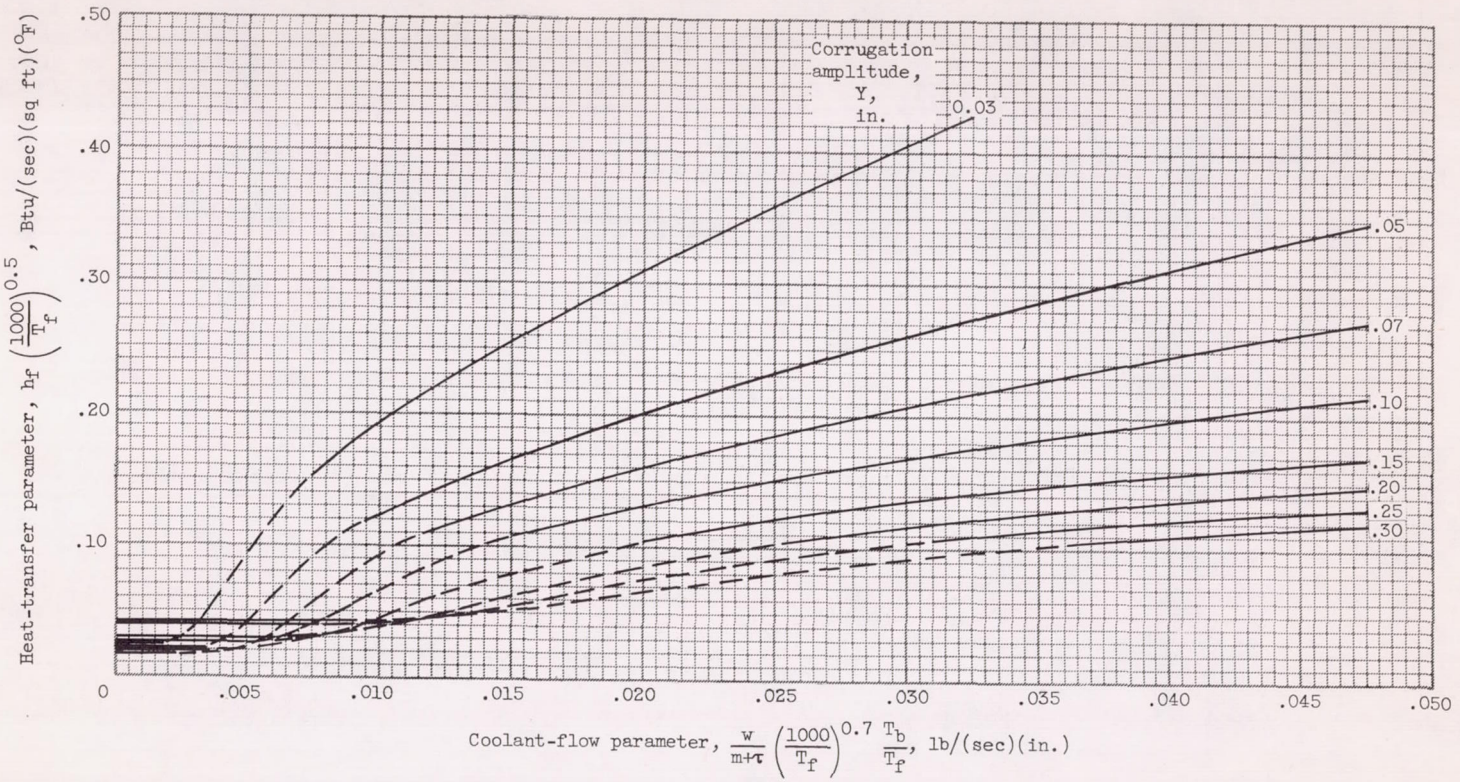

(h) Fin spacing, 0.050 inch; fin thickness, 0.010 inch.

Chart II. - Continued. Variation of heat-transfer parameter with coolant-flow parameter for $\left(\frac{16}{K}\right)\left(\frac{T_f}{1000}\right)^{0.5} = 1.0$.

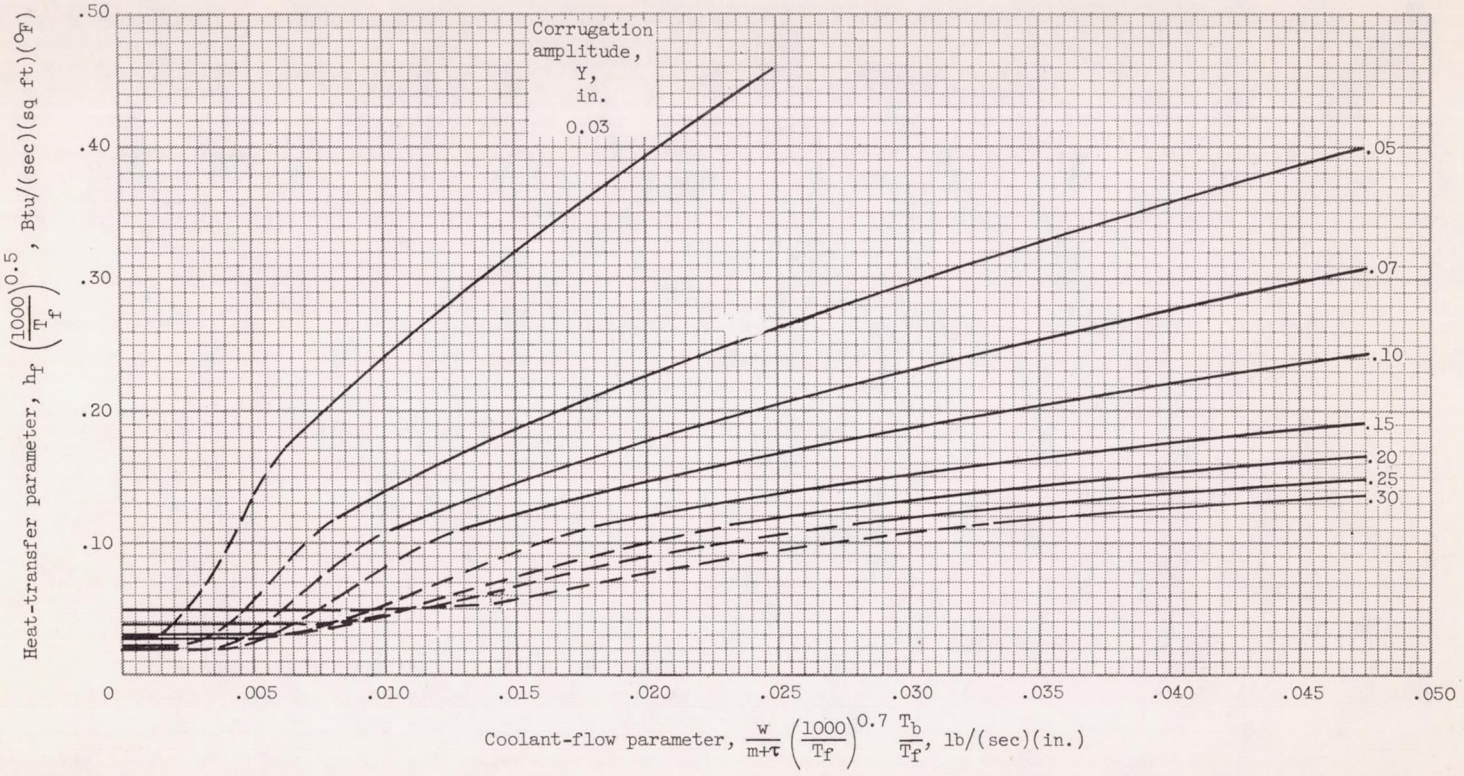

(i) Fin spacing, 0.050 inch; Fin thickness, 0.015 inch.

Chart II. - Concluded. Variation of heat-transfer parameter with coolant-flow parameter for $\left(\frac{16}{K}\right)\left(\frac{T_f}{1000}\right)^{0.5} = 1.0$.

Chart III

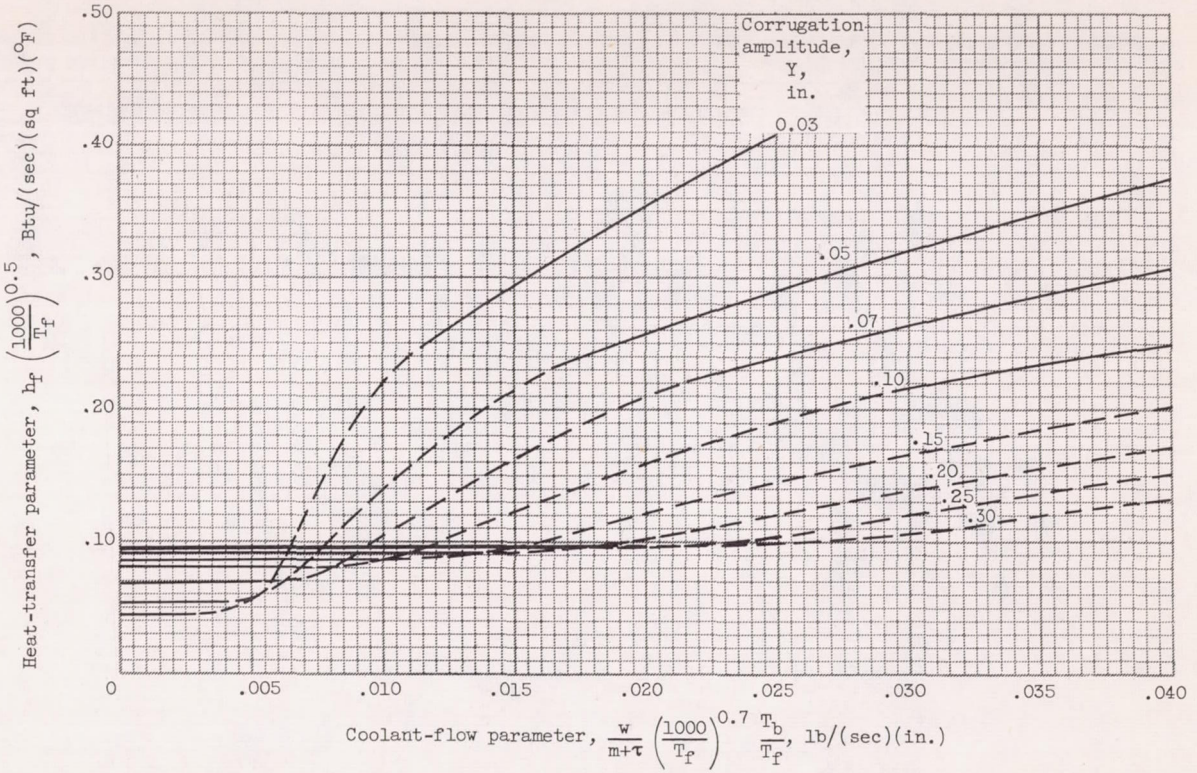

(a) Fin spacing, 0.020 inch; fin thickness, 0.005 inch.

Chart III. - Variation of heat-transfer parameter with coolant-flow parameter for $\left(\frac{16}{K}\right)\left(\frac{T_f}{1000}\right)^{0.5} \approx 2.0$.

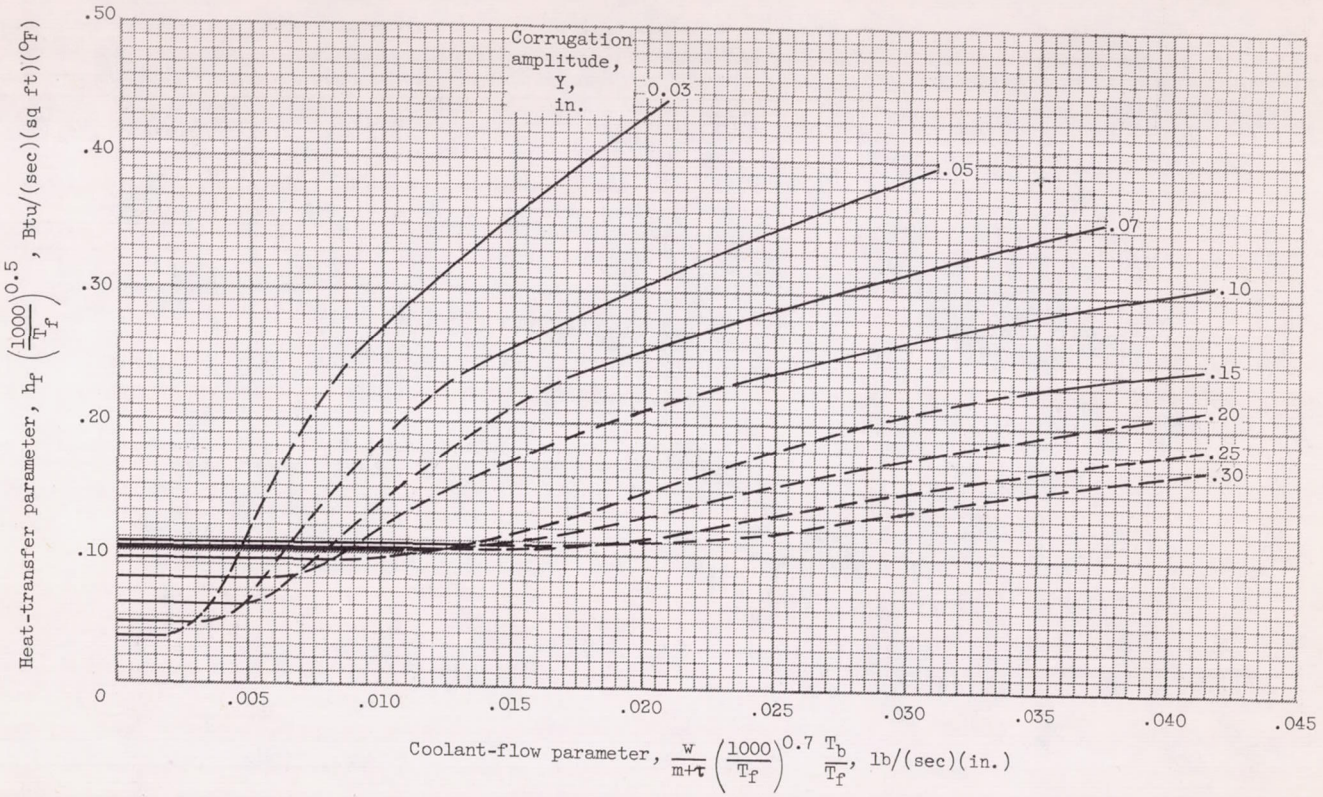

(b) Fin spacing, 0.020 inch; fin thickness, 0.010 inch.

Chart III. - Continued. Variation of heat-transfer parameter with coolant-flow parameter for $\left(\frac{16}{K}\right)\left(\frac{T_f}{1000}\right)^{0.5} = 2.0$.

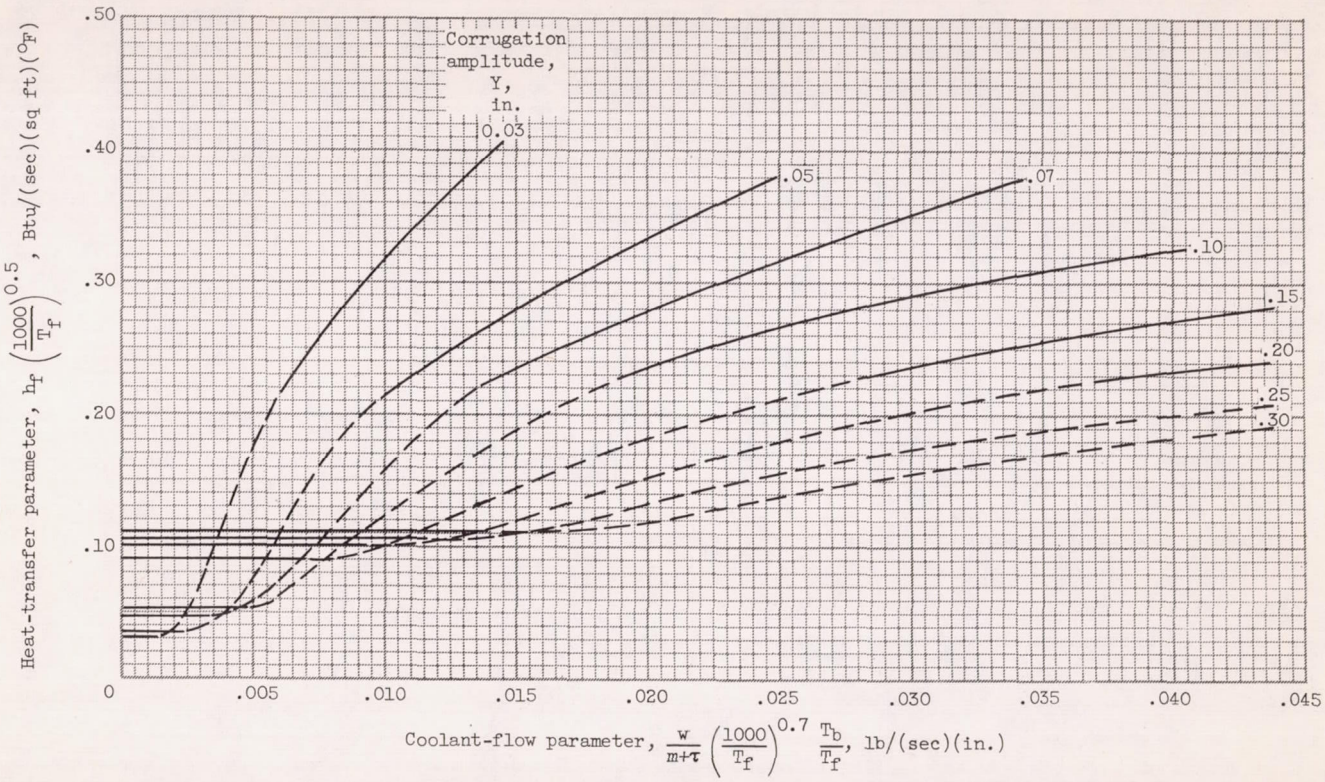

(c) Fin spacing, 0.020 inch; fin thickness, 0.015 inch.

Chart III. - Continued. Variation of heat-transfer parameter with coolant-flow parameter for $\left(\frac{16}{K}\right)\left(\frac{T_f}{1000}\right)^{0.5} = 2.0$.

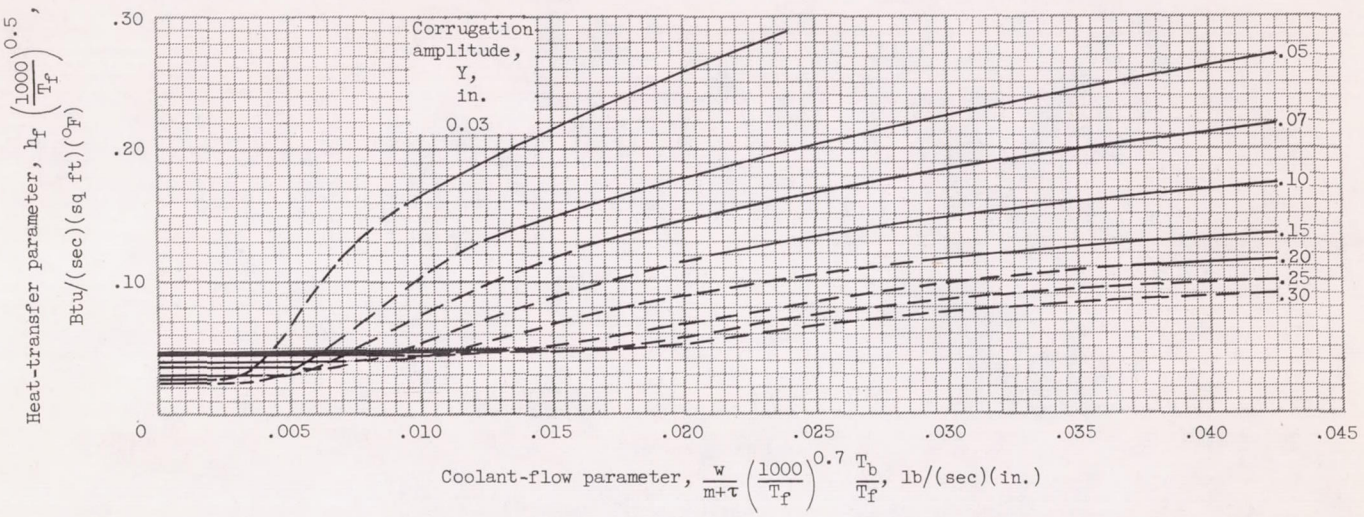

(d) Fin spacing, 0.035 inch; fin thickness, 0.005 inch.

Chart III. - Continued. Variation of heat-transfer parameter with coolant-flow parameter for $\left(\frac{16}{K}\right)\left(\frac{T_f}{1000}\right)^{0.5} = 2.0$.

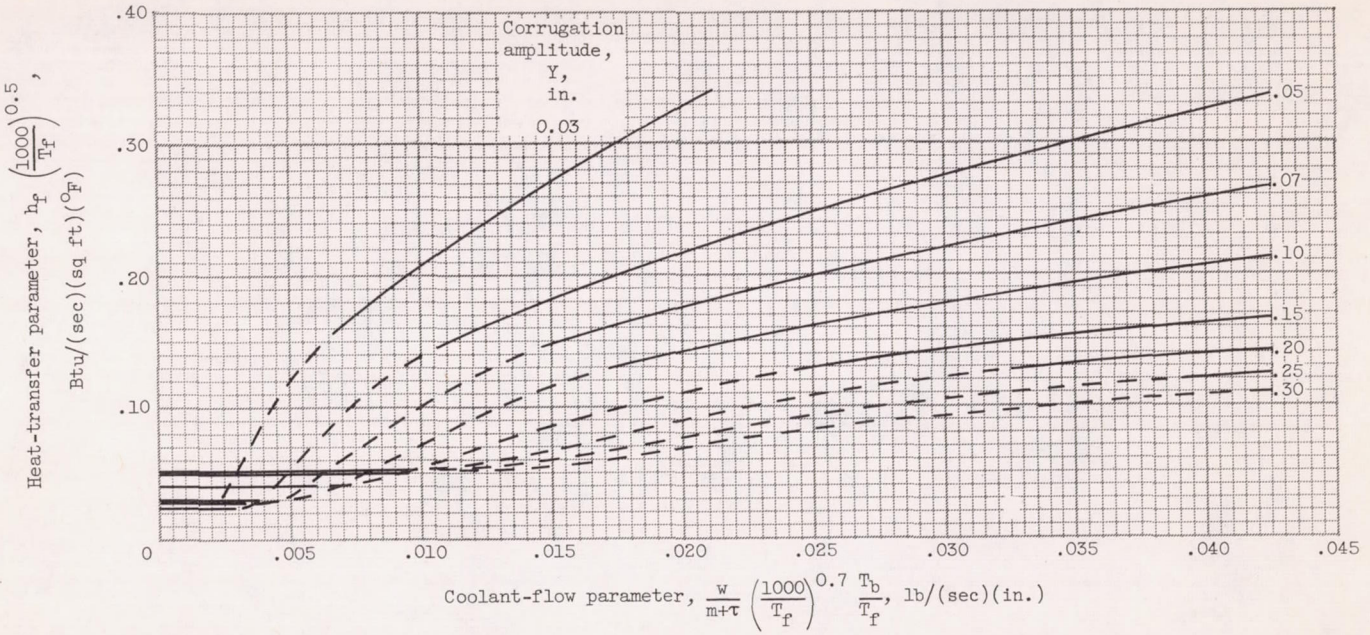

(e) Fin spacing, 0.035 inch; fin thickness, 0.010 inch.

Chart III. - Continued. Variation of heat-transfer parameter with coolant-flow parameter for $\left(\frac{16}{K}\right)\left(\frac{T_f}{1000}\right)^{0.5} = 2.0$.

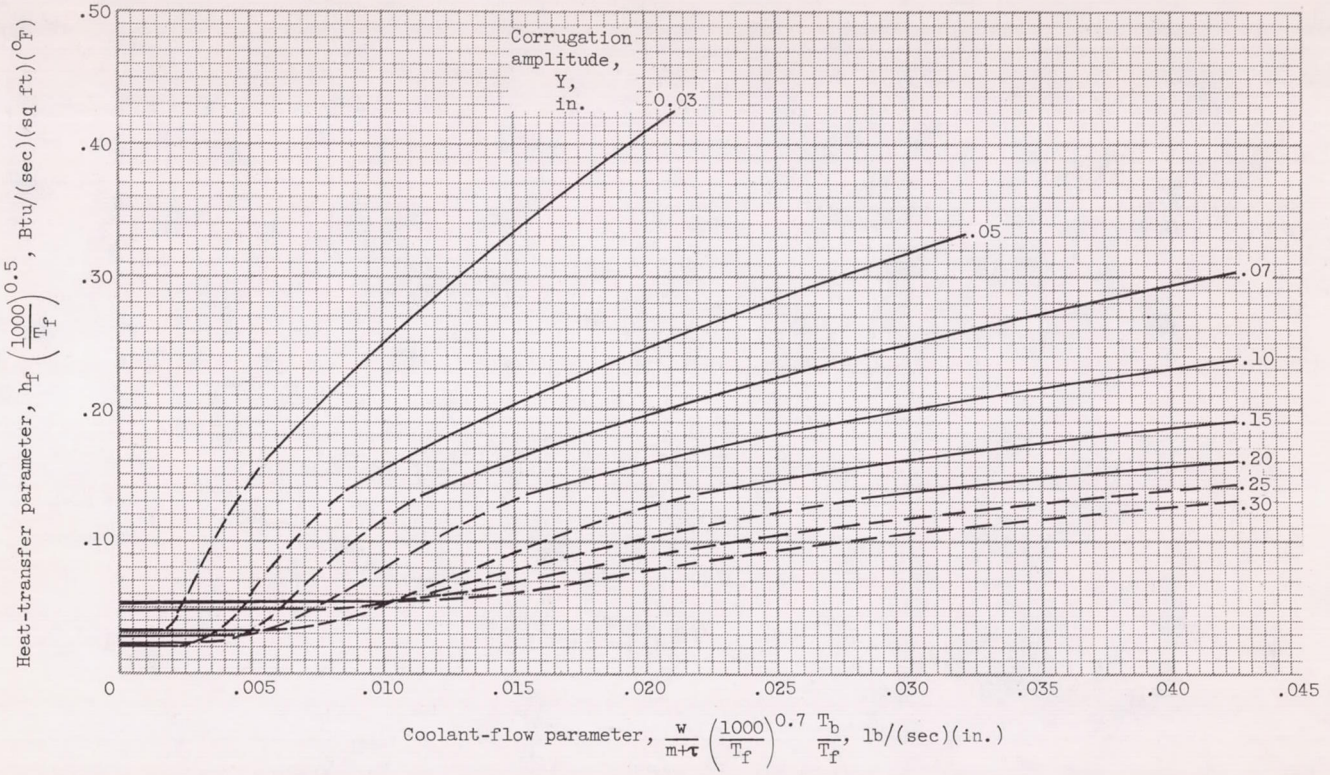

(f) Fin spacing, 0.035 inch; fin thickness, 0.015 inch.

Chart III. - Continued. Variation of heat-transfer parameter with coolant-flow parameter for $\left(\frac{16}{K}\right)\left(\frac{T_f}{1000}\right)^{0.5} = 2.0$.

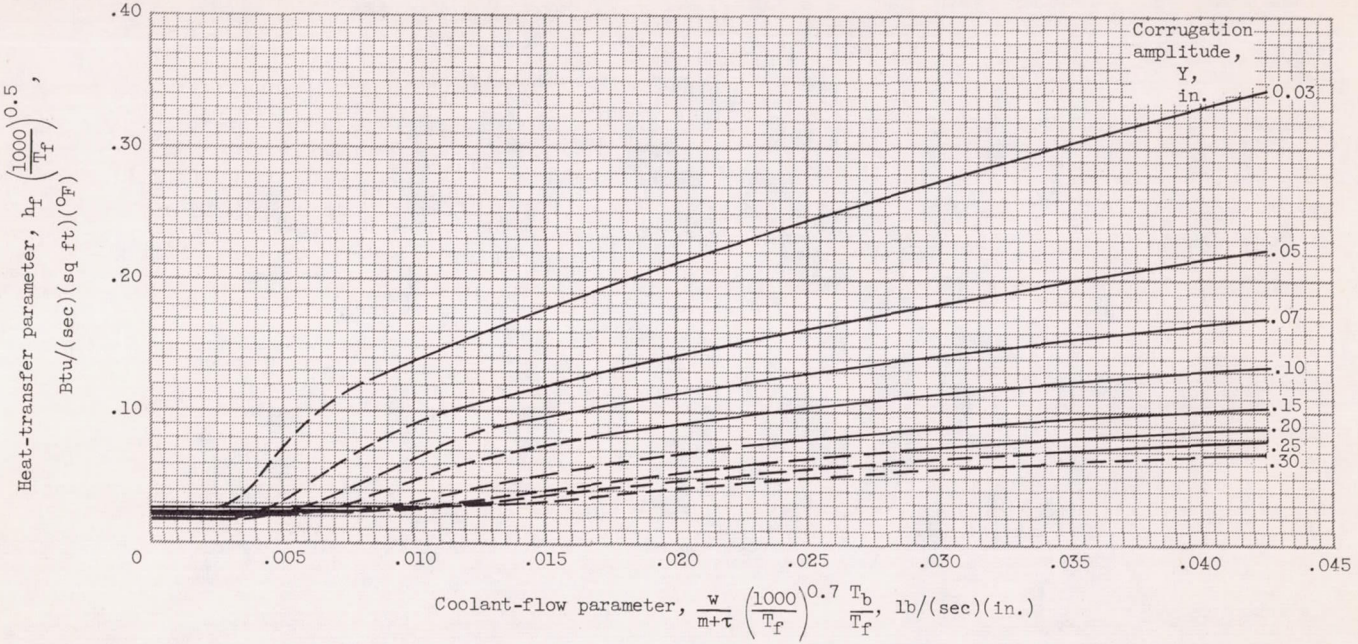

(g) Fin spacing, 0.050 inch; fin thickness, 0.005 inch.

Chart III. - Continued. Variation of heat-transfer parameter with coolant-flow parameter for $\left(\frac{16}{K}\right)\left(\frac{T_f}{1000}\right)^{0.5} = 2.0$.

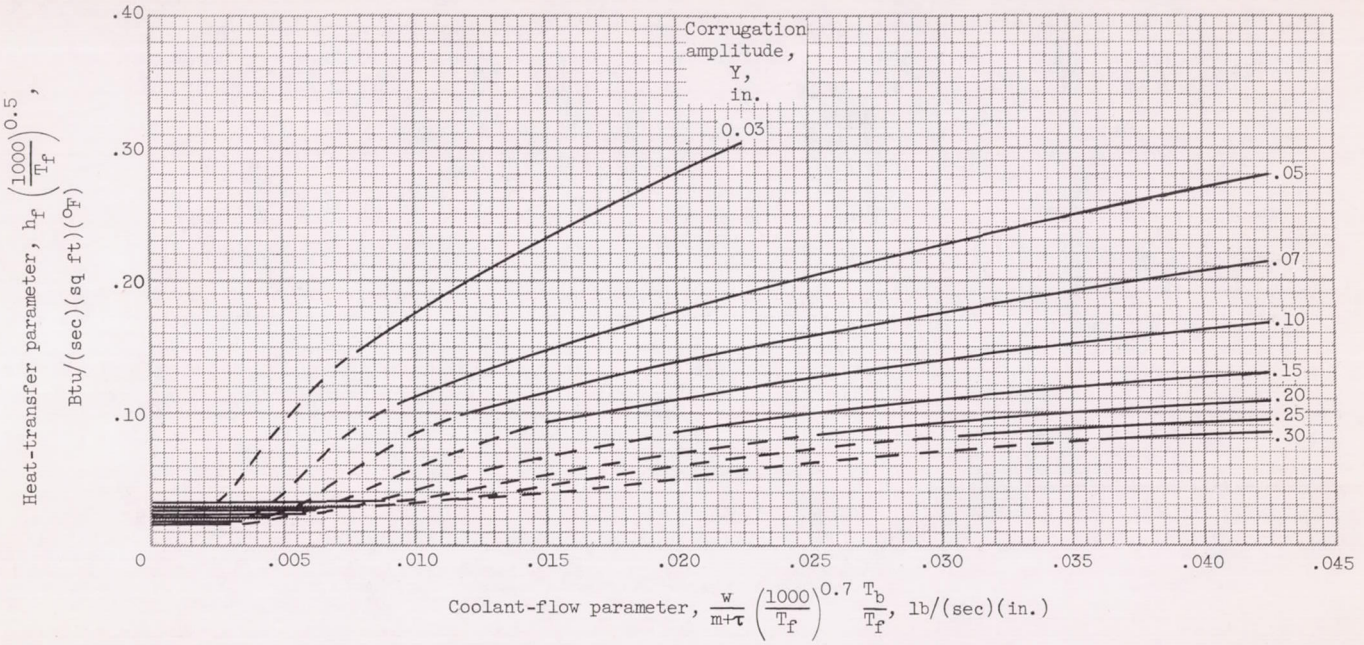

(h) Fin spacing, 0.050 inch; fin thickness, 0.010 inch.

Chart III. - Continued. Variation of heat-transfer parameter with coolant-flow parameter for $\left(\frac{16}{K}\right)\left(\frac{T_f}{1000}\right)^{0.5} = 2.0$.

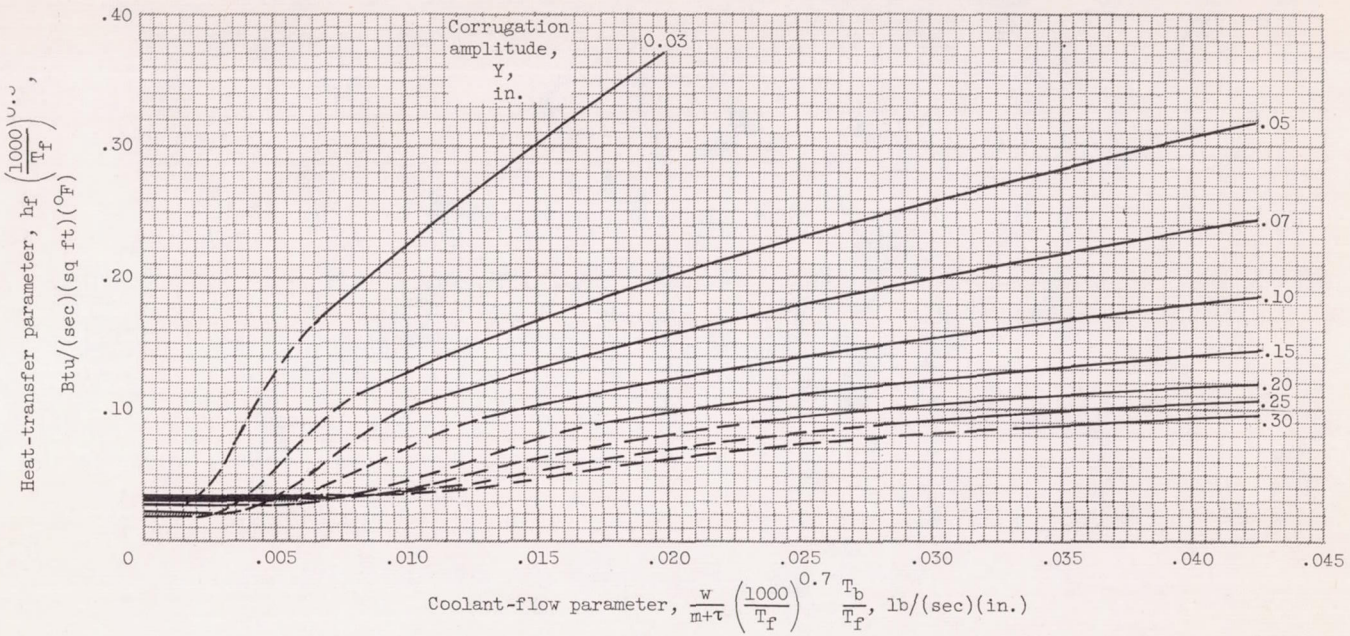

(i) Fin spacing, 0.050 inch; fin thickness, 0.015 inch.

Chart III. - Concluded. Variation of heat-transfer parameter with coolant-flow parameter for $\left(\frac{16}{K}\right)\left(\frac{T_f}{1000}\right)^{0.5} = 2.0$.

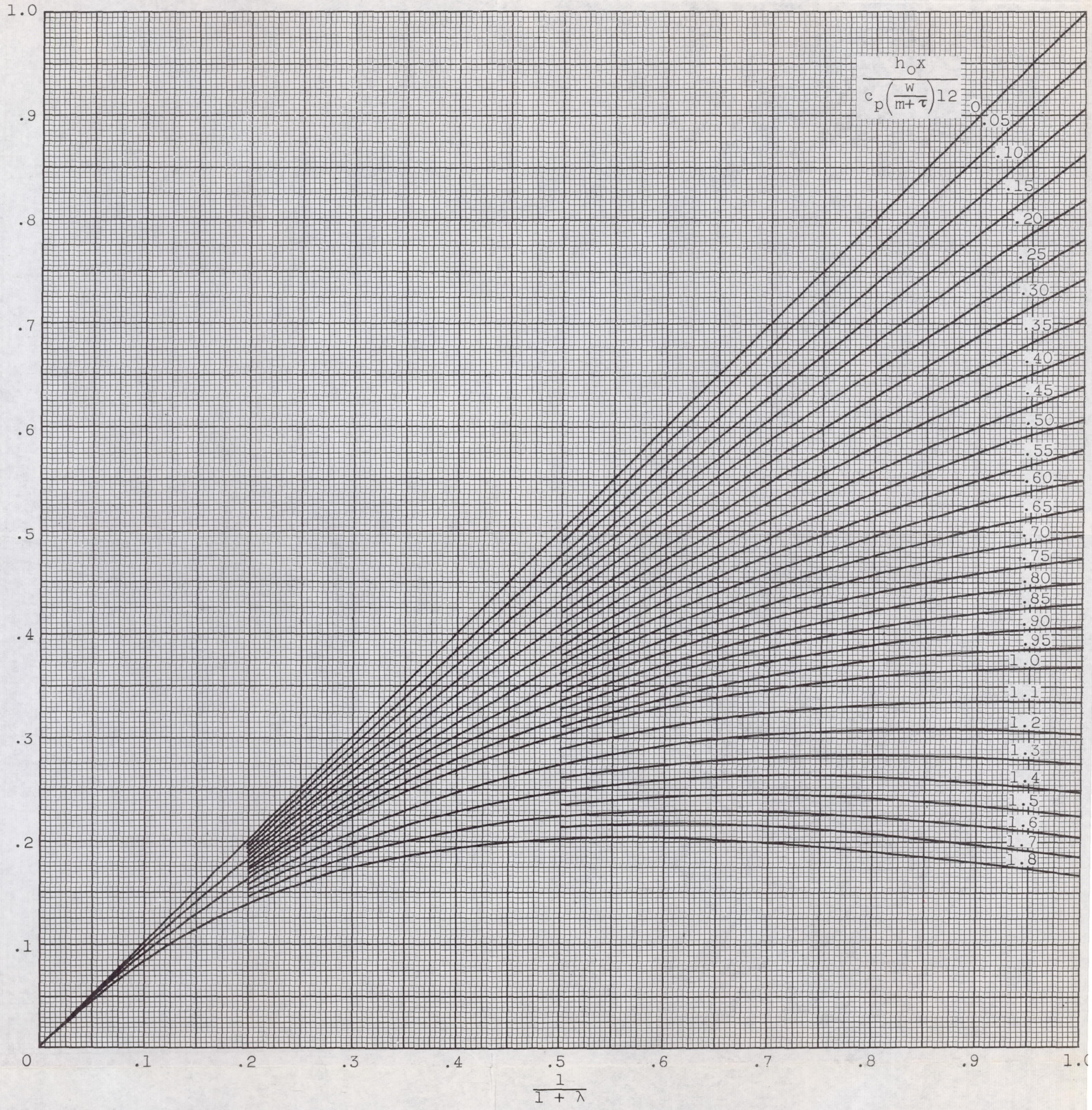

Figure 4. - Plot for evaluation of λ.